Human Molecular Genetics, 2012, Vol. 21, No. 11 **2432–2449**
doi:10.1093/hmg/dds058
Advance Access published on February 21, 2012

Suppression of α-synuclein toxicity and vesicle trafficking defects by phosphorylation at S129 in yeast depends on genetic context

Vicente Sancenon[1], Sue-Ann Lee[1,2], Christina Patrick[5], Janice Griffith[6], Amy Paulino[5], Tiago F. Outeiro[7,8], Fulvio Reggiori[6], Eliezer Masliah[5] and Paul J. Muchowski[1,2,3,4,*]

[1]Gladstone Institute of Neurological Disease, 1650 Owens Street, San Francisco, CA 94158, USA, [2]Biomedical Sciences Graduate Program, [3]Department of Biochemistry and Biophysics and [4]Department of Neurology, University of California, San Francisco, USA, [5]Department of Pathology and Medicine, University of California, San Diego, La Jolla, CA 92093, USA, [6]Department of Cell Biology, University Medical Center Utrecht, Utrecht, CX 3584, The Netherlands, [7]Cellular and Molecular Neuroscience Unit and [8]Instituto de Medicina Molecular, Instituto de Fisiologia, Faculdade de Medicina da Universidade de Lisboa, Lisboa, Portugal

Received November 16, 2011; Revised January 27, 2012; Accepted February 16, 2012

The aggregation of α-synuclein (αSyn) is a neuropathologic hallmark of Parkinson's disease and other synucleinopathies. In Lewy bodies, αSyn is extensively phosphorylated, predominantly at serine 129 (S129). Recent studies in yeast have shown that, at toxic levels, αSyn disrupts Rab homeostasis, causing an initial endoplasmic reticulum-to-Golgi block that precedes a generalized trafficking collapse. However, whether αSyn phosphorylation modulates trafficking defects has not been evaluated. Here, we show that constitutive expression of αSyn in yeast impairs late-exocytic, early-endocytic and/or recycling trafficking. Although members of the casein kinase I (CKI) family phosphorylate αSyn at S129, they attenuate αSyn toxicity and trafficking defects by an S129 phosphorylation-independent mechanism. Surprisingly, phosphorylation of S129 modulates αSyn toxicity and trafficking defects in a manner strictly determined by genetic background. Abnormal endosome morphology, increased levels of the endosome marker Rab5 and co-localization of mammalian CKI with αSyn aggregates are observed in brain sections from αSyn-overexpressing mice and human synucleinopathies. Our results contribute to evidence that suggests αSyn-induced defects in endocytosis, exocytosis and/or recycling of vesicles involved in these cellular processes might contribute to the pathogenesis of synucleinopathies.

INTRODUCTION

Synucleinopathies comprise a subset of neurodegenerative disorders characterized by the accumulation of cytoplasmic inclusions, or Lewy bodies (LBs), that contain the protein α-synuclein (αSyn) in selected populations of neurons [Parkinson's disease (PD) and dementia with Lewy bodies (DLB)] or glia [multiple system atrophy (MSA)]. Although the etiology of these disorders is unknown, the discovery of mutations in the αSyn gene (*SNCA*) that cause PD implicates αSyn in the pathogenesis of synucleinopathies (1).

The precise cellular function of αSyn is unclear. αSyn is a pre-synaptic protein that stimulates the formation of synaptic vesicles and neuronal transmission *in vitro* and *in vivo* (2–5). Importantly, the discovery that multiplications of the αSyn locus cause PD suggests that neurotoxicity is a quantitative trait of αSyn (6). Therefore, overexpression of αSyn has been widely used to study the molecular mechanisms of disease pathogenesis in a variety of model systems. In addition to other phenotypes, overexpression of αSyn appears to disrupt vesicular transport in cell-based and *in vitro* models, and in patients with PD (7–11). Yeast has proven useful as model to reconstitute αSyn dose-dependent cellular toxicity and vesicular transport defects. αSyn was shown to block ER-to-Golgi transport (12) and other intracellular trafficking pathways (13,14) at toxic concentrations. These trafficking

*To whom correspondence should be addressed. Tel: +1 4157342515; Fax: +1 4153550824; Email: pmuchowski@gladstone.ucsf.edu

failures correlate with an accumulation of intracellular vesicles (13,15). Interestingly, αSyn toxicity in yeast and other model organisms can be modulated by manipulating the expression of genes involved in vesicular trafficking (12,16–20).

Posttranslational modifications of αSyn *in vivo* may play an important role in the pathogenesis of PD and other synucleinopathies. The most abundant modification of αSyn in LBs is the phosphorylation of serine 129 (S129) (21,22). This residue is located within a casein kinase (CK) consensus recognition site and is phosphorylated by yeast and mammalian CKs (14,22–24) and other kinases (25–28) in cellular and animal models. However, the relevance of S129 phosphorylation for pathogenesis remains controversial. Discordant studies in rats and *Drosophila* argue for protective, innocuous and detrimental effects of phosphorylation on neurodegeneration (29–32). Moreover, whether phosphorylation influences αSyn-induced intracellular trafficking defects has not been evaluated.

In this study, we show that late-exocytic, early-endocytic and/or recycling transport of plasma membrane (PM) proteins is disrupted by constitutive expression of αSyn in yeast. Yeast casein kinase 1 (Yck1) attenuates this defect by a phosphorylation-independent mechanism. However, blocking αSyn phosphorylation dramatically enhances αSyn toxicity and trafficking defects in a strain-specific manner in yeast, suggesting that genetic context determines the sensitivity to changes in the phosphorylation state of αSyn. We also report early endosome (EE) alterations and co-localization of mammalian CKIδ with αSyn-positive inclusions in mouse models and human synucleinopathy brains, providing evidence that endosome anomalies and CKIδ sequestration may contribute to the pathogenesis of synucleinopathies.

RESULTS

Overexpression of αSyn causes vesicles to accumulate in yeast

Wild-type (WT) αSyn-GFP ectopically expressed in yeast from the galactose-inducible promoter of the *GAL1* gene accumulates in intracellular deposits that were initially described as inclusions (33). The earliest inclusions form at 3.5 h of induction in the cell periphery and subsequently spread toward the cell interior (13). Immuno-electron microscopy (IEM) studies revealed that the inclusions observed by fluorescence microscopy are composed of αSyn-positive clusters of vesicles (13,15). To further investigate the composition of these clusters, we examined the ultrastructure and the subcellular localization of αSyn by IEM over time in yeast expressing αSyn-GFP by the *GAL1* promoter. Within the first 4 h of induction, αSyn-GFP immunoreactivity was almost exclusively observed at the PM (data not shown). At 6 h, we observed small clusters of vesicles in the vicinity of the PM (Supplementary Material, Fig. S1A and B). The vesicles were homogeneous in size (∼20–40 nm in diameter), morphology and electron density, suggesting a common origin. At 12 h, the clusters were enlarged, and their vesicular content became heterogeneous in morphology and size (up to ∼100 nm in diameter), consistent with multiple origins of vesicles due to a widespread trafficking defect as reported (13) (Supplementary Material, Fig. S1C and D). Notably, αSyn-GFP immunoreactivity was detected on the surface of the vesicles at 6 and 12 h, in agreement with previous reports showing that the αSyn inclusions observed by fluorescence microscopy correspond to these clusters of αSyn-positive vesicles.

Constitutive αSyn expression disrupts late-exocytic, early-endocytic and/or recycling trafficking in yeast

Although the Lindquist group initially showed that αSyn inclusions co-localize with Ypt1, an endoplasmic reticulum (ER)-to-Golgi trafficking marker (12), a follow-up study by the same group showed co-localization with diverse trafficking markers, including Ypt31 (late Golgi), Sec4 (secretory vesicles-to-PM), Ypt6 (endosome-to-Golgi), Vps21 and Ypt52 [EE-to-late endosome (LE)] and Ypt7 (LE-to-vacuole), suggesting that αSyn may disrupt multiple intracellular trafficking routes in yeast (13). To investigate the precise origin of vesicles that accumulate after αSyn expression in yeast, we evaluated the effect of constitutively expressing untagged αSyn from a glycerol-3-phosphate dehydrogenase (*GPD1*) promoter in a 2 μm plasmid on the steady-state localization of a series of GFP-tagged protein markers for different intracellular trafficking pathways (34–36) (Fig. 1A). GFP-Snc1, a transmembrane exocytic SNARE (soluble *N*-ethylmaleimide-sensitive factor attachment protein receptor), is targeted to the PM through the secretory pathway and subsequently recycled to the PM via EEs and the Golgi. Ste2-GFP, the transmembrane α-factor pheromone receptor, and GFP-Snc1-Sso1, an engineered variant of GFP-Snc1 containing a transmembrane domain of the SNARE Sso1, are targeted to the PM through the secretory pathway and, subsequently, after endocytosis, to the vacuolar lumen via EE and LEs. The SNARE GFP-Pep12 is targeted to the membrane of the prevacuolar complex (PVC) via the carboxypeptidase Y (CPY) biosynthetic pathway (ER to Golgi to PVC/LE to vacuole). The transmembrane proteins GFP-Phm5 and Sna3-GFP are targeted to the vacuolar lumen via the CPY pathway by ubiquitin-dependent and -independent mechanisms, respectively. GFP-Nyv1-Snc1, an engineered variant of the SNARE Nyv1 containing the transmembrane domain of Snc1, is targeted to the vacuole membrane via the alkaline phosphatase (ALP) pathway (ER to Golgi to vacuole).

To quantitatively assess the effect of αSyn on trafficking, we counted the percentage of cells that exhibit a mislocalization phenotype, considered as any anomaly in the localization pattern of a trafficking marker that differs from the pattern displayed by the majority of cells that do not express αSyn. Constitutive expression of untagged αSyn from the *GPD1* promoter selectively prevented the proper targeting of GFP-Snc1 to the PM and of GFP-Snc1-Sso1 and Ste2-GFP to the vacuole lumen in ∼50–85% of cells, but not of GFP-Pep12 and GFP-Nyv1-Snc1 to the vacuole membrane or GFP-Phm5 and Sna3-GFP to the vacuole lumen (Fig. 1B and C). The trafficking routes that are unique to the protein markers perturbed by untagged αSyn include Golgi-to-PM, PM-to-endosome and endosome-to-Golgi. These observations suggest that, at the steady-state expression levels achieved by the *GPD1* promoter, untagged αSyn impairs the delivery of proteins to the PM from the Golgi and/or their subsequent

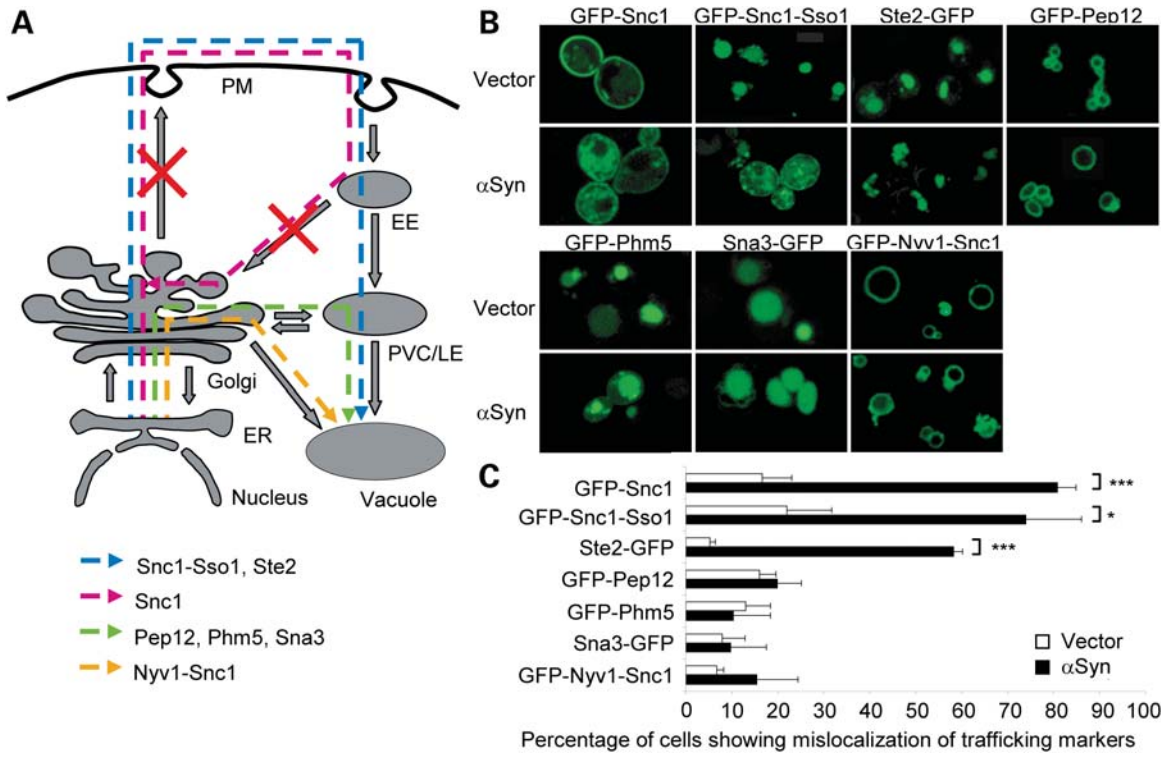

Figure 1. Untagged αSyn overexpression causes the mislocalization of late-exocytic and early-endocytic protein markers. (**A**) Schematic representation of the trafficking routes of the indicated protein markers in yeast. Red crosses indicate putative trafficking steps blocked by constitutive αSyn expression. EE, early endosome; ER, endoplasmic reticulum; PM, plasma membrane; PVC/LE, prevacuolar complex/late endosome. (**B**) Effect of untagged αSyn on the localization of the indicated protein trafficking markers. BY4741 strain co-transformed with plasmids for the expression of the indicated protein markers, and untagged WT αSyn under the control of a *GPD1* constitutive promoter or the corresponding empty vector was imaged in the logarithmic phase. (**C**) Quantification of the percentage of cells from (B) exhibiting mislocalization of the indicated trafficking markers. Error bars represent the standard deviation of three experiments. $^{*}P < 0.05$; $^{**}P < 0.01$; $^{***}P < 0.001$; Student's *t*-test.

endocytic and recycling trafficking. In contrast, other markers that use the ER-to-Golgi pathway but bypass the PM (GFP-Pep12, GFP-Phm5, Sna3-GFP and GFP-Nyv1-Snc1) do not exhibit localization defects in αSyn-expressing cells, suggesting that ER-to-Golgi trafficking is not impaired.

We next analyzed the subcellular distribution of αSyn-GFP and the exocytic SNARE Snc1 by co-IEM (Fig. 2). Consistent with the fluorescence microscopy studies, Snc1 immunoreactivity was detected in the αSyn-GFP-positive vesicular clusters, confirming anomalies in PM delivery, endocytic and/or recycling trafficking of Snc1. As αSyn has been reported to block the delivery of the dye FM 4-64 to the vacuole, but not its uptake (33), we propose that αSyn impairs post-endocytic and/or recycling trafficking that follows vesicle budding from the PM (Fig. 1A), at least at early stages after expression.

To gain further insights in the trafficking steps disrupted by αSyn, we investigated the subcellular distribution of GFP-Snc1-Sso1 and the dye FM 4-64 in two subsets of yeast trafficking mutants (Supplementary Material, Fig. S2A): first, in loss-of-function deletion mutants defective in intra-Golgi (*ypt31*Δ), endocytic (*end3*Δ, *ypt51*Δ), recycling (*ypt31*Δ), endosome-to-Golgi (*vps35*Δ) and endosome-to-vacuole (*vps23*Δ, *did3*Δ) transport, endosome and vacuole homotypic fusion (*ypt7*Δ) and actin remodeling (*sac6*Δ); second, in temperature-sensitive secretory mutants defective in ER-to-Golgi (*sec7-4*, *sec18-1*), intra-Golgi (*sec7-4*) and Golgi-to-PM (*sec1-1*) transport at permissive [room temperature (RT)] and non-permissive (37°C) temperatures. Among all of the mutants studied, *did3*Δ and *vps23*Δ appear to most closely resemble the mislocalization pattern of GFP-Snc1-Sso1 caused by αSyn, suggesting a late-endocytic defect (Supplementary Material, Fig. S2B and C). However, the mislocalization phenotype in αSyn-expressing cells seems to rather be unique, suggesting that multiple trafficking steps are affected, in agreement with a previous study (13).

Yck1 attenuates αSyn-induced toxicity and trafficking defects through an S129 phosphorylation-independent mechanism

There is increasing evidence that αSyn disrupts endocytic trafficking. For example, in yeast αSyn overexpression perturbs the subcellular distribution of the endocytic tracker FM 4-64 (33) and diverse endocytic protein markers (13). The endocytic pathway modulates αSyn toxicity in *Caenorhabditis elegans* (17). Therefore, we reasoned that genes that regulate endocytosis might also modify αSyn-induced growth defects and vesicle accumulation in yeast. To test this hypothesis, we assessed whether Yck1 and Yck2, two functionally redundant PM-associated members of the CKI protein family that promote the endocytosis of PM proteins (37,38), modulate

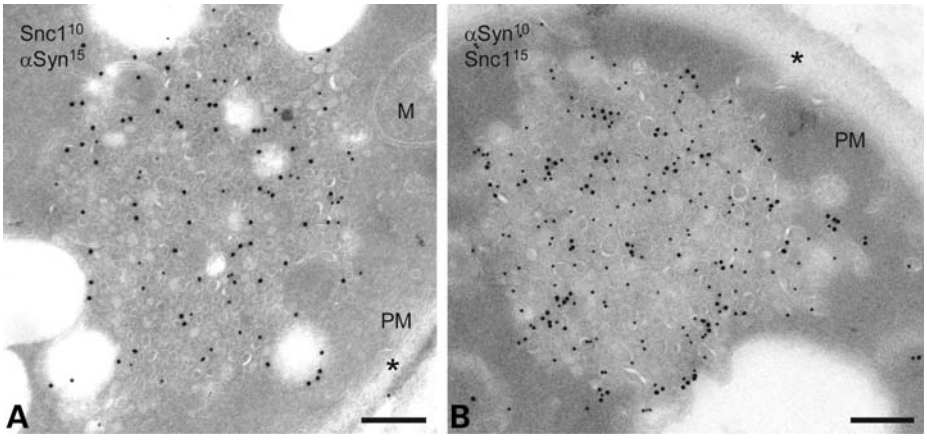

Figure 2. αSyn-induced vesicular clusters contain the exocytic SNARE Snc1. Strain FRY346 carrying an integrated *8xMYC-SNC1* fusion and transformed with a plasmid for the expression of αSyn-GFP under the control of a constitutive *GPD1* promoter was grown to the logarithmic phase, and cells were processed for IEM. In the left panel (**A**), cryosections were first incubated with anti-myc antibodies and then with anti GFP antibodies (αSyn^{15}, 15 nm gold particles; $Snc1^{10}$, 10 nm gold particles), whereas in the right panel (**B**) the sequence of the antibodies was inverted (αSyn^{10}, 10 nm gold; $Snc1^{15}$, 15 nm gold particles). PM, plasma membrane; M, mitochondria. The asterisk denotes the cell wall. Bar, 200 nm.

αSyn toxicity. For these studies, we generated a yeast strain carrying two stably integrated copies of the human αSyn gene fused to GFP under the control of the *GAL1* inducible promoter (which allows to control for gene-specific effects in non-inducing conditions) in the BY4741 strain (Table 1). As positive and negative controls, we deleted the genes *TLG2*, a known αSyn toxicity modifier encoding a SNARE required for the targeting of Yck2 to the PM (20,39), and *SPO14*, a gene encoding a yeast phospholipase D that does not modify αSyn toxicity (40), respectively. In contrast to a previous study (14), we found that deletion of *YCK1* and *YCK2* genes significantly increased the growth defect caused by αSyn-GFP (Fig. 3A and Supplementary Material, Fig. S3).

To confirm these genetic interactions, we reasoned that pharmacologic inhibition of CKI activity in yeast expressing αSyn should phenocopy the *yck1*Δ or *yck2*Δ alleles, and this effect should be more dramatic in yeast lacking either one of the two functionally redundant enzymes. Therefore, we tested the effect of the CKI-specific inhibitor D4476 on the viability of cells expressing αSyn-GFP from two genomic loci. To make cells more sensitive to the compound, we knocked out the multidrug resistance gene *PDR1* in all the strains tested. Although *YCK1* or *YCK2* are not individually essential for cell growth, deletion of both genes results in growth arrest. As expected, the CKI-specific inhibitor D4476 decreased yeast growth in a concentration-dependent manner (Supplementary Material, Fig. S4). Notably, this effect was more pronounced in cells expressing αSyn-GFP, and was significantly increased in cells lacking one of the two redundant enzymes (Supplementary Material, Fig. S4), suggesting that CKI activity counteracts the detrimental effects of αSyn overload.

To determine whether the increase in growth inhibition caused by the loss of CKI function correlates with increased trafficking defects, we studied the localization of mCherry-tagged Snc1-Sso1 in WT and *yck1*Δ cells carrying two or zero integrated copies of the galactose-inducible αSyn-GFP gene. In cells not expressing αSyn-GFP, mCherry-Snc1-Sso1 is correctly delivered to the vacuolar lumen (Fig. 3B). In contrast, expression of αSyn-GFP prevented the proper targeting of mCherry-Snc1-Sso1 in ∼30% of WT cells (Fig. 3B and C). Note that the defect in these cells is less marked than in cells constitutively expressing untagged αSyn from a 2 μm plasmid, where ∼75% of cells are affected (Fig. 1C). However, deletion of *YCK1* did not aggravate this phenotype (Fig. 3B and C), indicating that the enhancement of growth defects by the *yck1*Δ mutation is not associated with an enhancement of endocytic trafficking defects.

Next, we investigated the ability of *YCK1* to reverse αSyn-induced toxicity and trafficking defects (Fig. 3D and E). We observed that *YCK1* overexpression attenuates the growth defect caused by two copies of the αSyn-GFP gene in WT and *yck1*Δ cells. In addition, in contrast to the absence of trafficking defect enhancement upon deletion of *YCK1*, overexpression of *YCK1* significantly reduced the percentage of cells showing abnormal localization of GFP-Snc1-Sso1 in cells constitutively expressing untagged αSyn (Fig. 3E). Interestingly, Ypt1, a Rab GTPase that also suppresses untagged αSyn toxicity (12), decreased mislocalization of GFP-Snc1-Sso1 to the same extent. These results suggest that Yck1 and Ypt1 may alleviate αSyn toxicity, at least in part, by directly promoting PM endocytosis.

αSyn contains a consensus CKI phosphorylation site on S129 that is phosphorylated by yeast and mammalian CKI *in vitro* and *in vivo* (14,24). To assess whether αSyn is phosphorylated at S129 in yeast, we monitored the levels of total and phosphorylated αSyn-GFP (pS129) over time in WT cells carrying two copies of the αSyn-GFP gene under the control of the *GAL1* promoter. Both αSyn and its phosphorylated form were detected after 1 h of inducing αSyn-GFP expression, indicating that αSyn is rapidly phosphorylated in yeast (Fig. 3F). To test whether CKI modulates directly or indirectly the phosphorylation of αSyn at S129 in our model, we compared the relative levels of pS129 in the WT, *yck1*Δ and *yck2*Δ strains after 1 h of induction. The *spo14*Δ strain was included as negative control. As shown previously (14), we

Table 1. Strains used in this study

Strain	MT[a]	Genotype	Source
BY4741	*MAT***a**	*his3Δ1 leu2Δ0 met15Δ0 ura3Δ0*	(75)
FRY346	*MAT***a**	BY4741 *TPI1pr-8xMYC-SNC1*::*URA3*	This study
Y5563	*MAT*α	*can1Δ*::*MFA1pr-HIS3 lyp1Δ his3Δ1 leu2Δ0 met15Δ0 ura3Δ0 LYS2+*	(76)
VSY1	*MAT***a**	BY4741 *ade2Δ0*::*SNCA*(WT)-*GFP NatR*	This study
VSY2	*MAT*α	Y5563 *trp1Δ0*::*SNCA*(WT)-*GFP URA3+*	This study
VSY4	*MAT*α	VSY2 *ade2Δ0*::*SNCA*(WT)-*GFP NatR*	This study
VSY17	*MAT***a**	VSY4 *yck1Δ0*::*KanR*	This study
VSY58	*MAT***a**	VSY4 *yck2Δ0*::*KanR*	This study
VSY59	*MAT***a**	VSY4 *tlg2Δ0*::*KanR*	This study
VSY60	*MAT***a**	VSY4 *spo14Δ0*::*KanR*	This study
yck1Δ	*MAT***a**	BY4741 *yck1Δ0*::*KanR*	(87)
yck2Δ	*MAT***a**	BY4741 *yck2Δ0*::*KanR*	(87)
spo14Δ	*MAT***a**	BY4741 *spo14Δ0*::*KanR*	(87)
tlg2Δ	*MAT***a**	BY4741 *tlg2Δ0*::*KanR*	(87)
pdr1Δ	*MAT***a**	BY4741 *pdr1Δ0*::*KanR*	(87)
did3Δ	*MAT***a**	BY4741 *did3Δ0*::*KanR*	(87)
end3Δ	*MAT***a**	BY4741 *end3Δ0*::*KanR*	(87)
rcy1Δ	*MAT***a**	BY4741 *rcy1Δ0*::*KanR*	(87)
sac6Δ	*MAT***a**	BY4741 *sac6Δ0*::*KanR*	(87)
vps23Δ	*MAT***a**	BY4741 *vps23Δ0*::*KanR*	(87)
vps35Δ	*MAT***a**	BY4741 *vps35Δ0*::*KanR*	(87)
ypt7Δ	*MAT***a**	BY4741 *ypt7Δ0*::*KanR*	(87)
ypt31Δ	*MAT***a**	BY4741 *ypt31Δ0*::*KanR*	(87)
ypt51Δ	*MAT***a**	BY4741 *ypt51Δ0*::*KanR*	(87)
RSY255	*MAT*α	*ura3-52 leu2-3,-112*	(88)
RY782	*MAT*α	*his4-619 ura3-52 sec1-1*	(88)
RY112	*MAT***a**	*his4-619 ura3-52 leu2-3,-112 trp1-289 sec 7-4*	(88)
RY271	*MAT*α	*his4-619 ura3-5 sec18-1*	(88)
VSY5	*MAT*α	VSY4 *pdr1Δ0*::*KanR*	This study
VSY24	*MAT***a**	VSY17 *yck1Δ0*::*kanRΔ0*::*LEU2*	This study
VSY25	*MAT***a**	VSY24 *pdr1Δ0*::*KanR*	This study
W303-1A	*MAT***a**	*can1-100 his3-11 15 leu2-3 112 trp1-1 ura3-1 ade2-1*	(89)
VSY67	*MAT***a**	W303-1A *ura3-1*::*pRS306 URA3+*	This study
VSY68	*MAT***a**	W303-1A *ura3-1*::*GAL1pr-SNCA*(WT)-*GFP URA3+*	This study
VSY69	*MAT***a**	W303-1A *ura3-1*::*GAL1pr-SNCA*(S129A)-*GFP URA3+*	This study
VSY70	*MAT***a**	W303-1A *ura3-1*::*GAL1pr-SNCA*(S129E)-*GFP URA3+*	This study
VSY71	*MAT***a**	VSY67 *trp1-1*::*pRS304 TRP1+*	This study
VSY72	*MAT***a**	VSY68 *trp1-1*::*GAL1pr-SNCA*(WT)-*GFP TRP1+*	This study
VSY73	*MAT***a**	VSY69 *trp1-1*::*GAL1pr-SNCA*(S129A)-*GFP TRP1+*	This study
VSY74	*MAT***a**	VSY70 *trp1-1*::*GAL1pr-SNCA*(S129E)-*GFP TRP1+*	This study
VSY75	*MAT***a**	VSY71 *yck1Δ0*::*KanR*	This study
VSY76	*MAT***a**	VSY72 *yck1Δ0*::*KanR*	This study
VSY77	*MAT***a**	VSY73 *yck1Δ0*::*KanR*	This study
VSY78	*MAT***a**	VSY74 *yck1Δ0*::*KanR*	This study
VSY79	*MAT*α	Y5563 *trp1Δ0*::*pRS405 LEU2+*	This study
VSY80	*MAT*α	Y5563 *trp1Δ0*::*SNCA*(WT)-*GFP LEU2+*	This study
VSY81	*MAT*α	Y5563 *trp1Δ0*::*SNCA*(S129A)-*GFP LEU2+*	This study
VSY82	*MAT*α	Y5563 *trp1Δ0*::*SNCA*(S129E)-*GFP LEU2+*	This study
VSY83	*MAT*α	VSY79 *pdr1Δ0*::*pRS465 URA3+*	This study
VSY84	*MAT*α	VSY80 *pdr1Δ0*::*SNCA*(WT)-*GFP URA3+*	This study
VSY85	*MAT*α	VSY81 *pdr1Δ0*::*SNCA*(S129A)-*GFP URA3+*	This study
VSY86	*MAT*α	VSY82 *pdr1Δ0*::*SNCA*(S129E)-*GFP URA3+*	This study

[a]Mating type.

observed a modest (∼30%) decrease in the relative levels of pS129 in the *yck1Δ* and *yck2Δ* mutants compared with the WT strain (Fig. 3G and H), confirming that CKI contributes partially to the phosphorylation of S129.

To determine whether the attenuation of growth and trafficking defects by Yck1 is mediated by direct phosphorylation of αSyn, we measured the levels of pS129 in WT and *yck1Δ* cells transformed with a plasmid for the overexpression of *YCK1* or the corresponding empty vector at 5.5 and 11 h of induction (Fig. 3I). As control, we treated cells with a combination of the phosphatase inhibitors (PI) okadaic acid and activated Na_3VO_4. *YCK1* overexpression did not increase αSyn phosphorylation in either WT or *yck1Δ* cells, suggesting that the attenuation of toxicity and trafficking defects by *YCK1* is not mediated by direct phosphorylation of αSyn at S129, but rather through the phosphorylation of other targets.

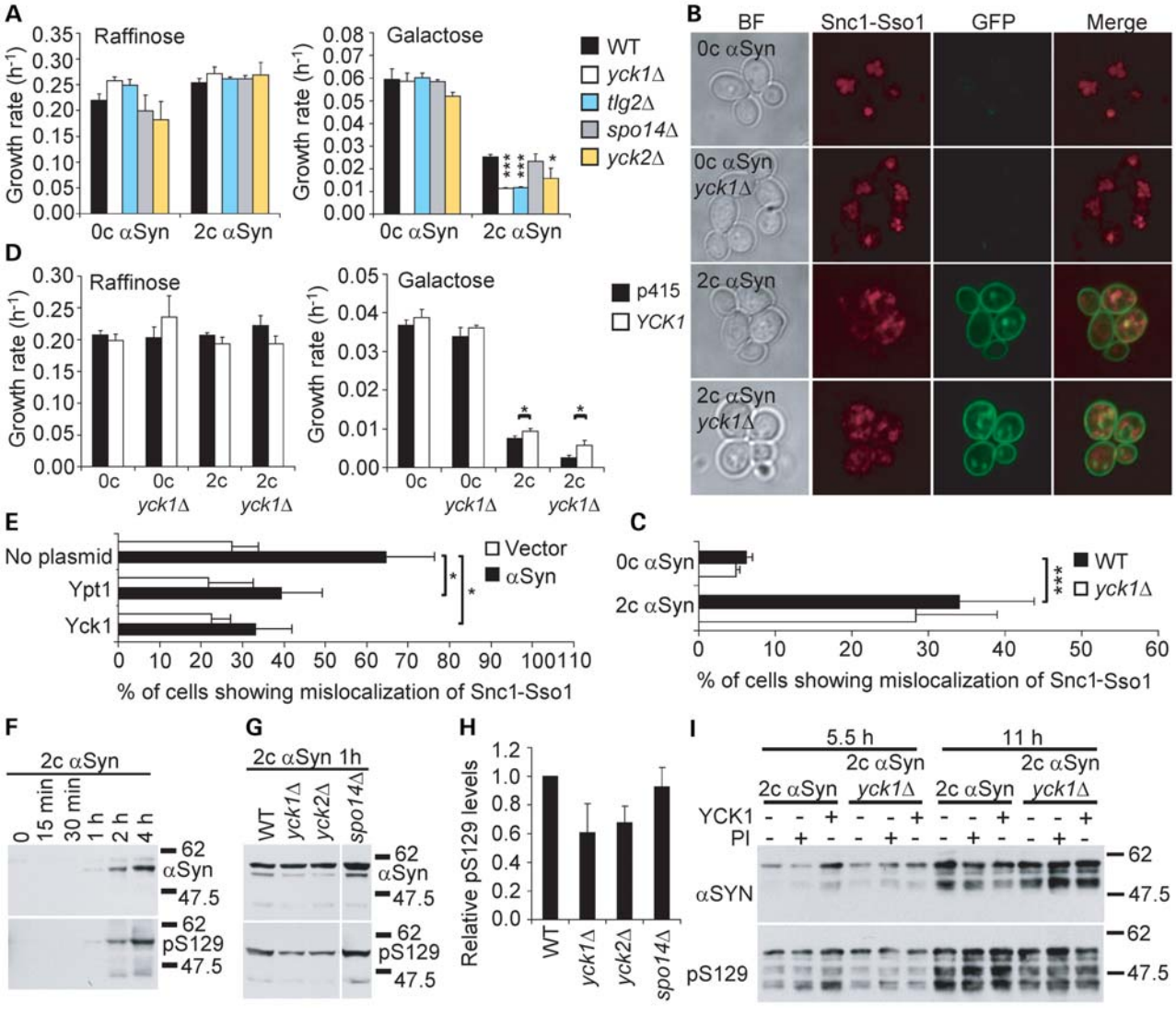

Figure 3. Yck1 attenuates αSyn-induced toxicity and trafficking defects through an S129 phosphorylation-independent mechanism. (**A**) Deletion of CKI genes (*yck1*Δ, *yck2*Δ) enhances the growth defect caused by αSyn overexpression in the BY4741 genetic background. Growth rates of WT cells or the indicated mutant strains containing either two copies (2c) or no copies (0c) of the αSyn-GFP gene in the BY4741 genetic background in conditions that do (galactose) or do not (raffinose) induce the expression of αSyn-GFP. The *tlg2*Δ and *spo14*Δ mutants are included as positive and negative controls, respectively. Growth rates were determined as the slope of the growth curves shown in Supplementary Material, Figure S3, during the logarithmic phase. (**B**) Deletion of *YCK1* does not enhance the defects in the trafficking of the marker Snc1-Sso1 caused by αSyn-GFP. WT or *yck1*Δ cells containing two copies (2c) or no copies (0c) of the αSyn-GFP gene in the BY4741 genetic background were transformed with a plasmid for the expression of trafficking marker mCherry-Snc1-Sso1, induced overnight in galactose-containing media and imaged in the logarithmic phase. (**C**) Quantification of the percentage of cells from (B) showing mislocalization of mCherry-Snc1-Sso1. (**D**) Overexpression of *YCK1* partially attenuates αSyn-induced growth defects. Growth rates of WT or *yck1*Δ cells containing two copies (2c) or no copies (0c) of the αSyn-GFP gene in the BY4741 genetic background and transformed with a plasmid for the overexpression of *YCK1* or the corresponding empty plasmid (p415). (**E**) Yck1 and Ypt1 partially restore targeting of GFP-Snc1-Sso1 to the vacuolar lumen. BY4741 cells expressing GFP-Snc1-Sso1 were transformed with either untagged WT αSyn under the control of a constitutive *GPD1* promoter or the corresponding empty vector and the indicated plasmids for the overexpression of *YPT1* or *YCK1*. After transfer to a galactose-containing medium, cells were imaged in the logarithmic phase. The percentage of cells exhibiting mislocalization of GFP-Snc1-Sso1 is shown. (**F**) Kinetics of αSyn induction and phosphorylation in WT cells containing two copies of the αSyn-GFP gene in the BY4741 genetic background. Cells were grown to the logarithmic phase ($OD_{600} \approx 0.8$) in raffinose-containing media and expression of αSyn was induced with galactose. Aliquots were collected at the indicated times and levels of phosphorylated (pS129) and total αSyn were analyzed by western blot. The soluble fraction is shown. The earliest αSyn was detected after 1 h of induction. (**G**) Deletion of *YCK1* or *YCK2* reduces αSyn phosphorylation modestly. The indicated strains were induced for 1 h and analyzed by western blot as described in (F). (**H**) Quantification of the S129 phosphorylation levels was estimated as the ratio of the band densities of phosphorylated relative to total αSyn from (G). (**I**) Overexpression of *YCK1* does not increase αSyn phosphorylation at S129. WT or *yck1*Δ cells containing two copies (2c) or no copies (0c) of the αSyn-GFP gene in the BY4741 genetic background and transformed with a plasmid for the overexpression of *YCK1* or the corresponding empty vector were grown to the logarithmic phase in raffinose-containing medium and induced with galactose. Aliquots were collected at the indicated times for western blot analysis. The indicated cultures were treated with the PI okadaic acid and activated Na_3VO_4 for 15 min before being collected. Error bars represent standard deviations from three experiments in (A), (C), (D) and (E) and two experiments in (H). $^{*}P < 0.05$; $^{**}P < 0.01$; $^{***}P < 0.001$; (A, C, D and E) Student's *t*-test.

Phosphorylation regulates the toxicity and trafficking defects caused by αSyn in a genetic context-dependent manner

The role of S129 phosphorylation in disease pathogenesis is unclear, as contradictory results have been published in different models (29–32,41,42). To investigate the effect of S129 phosphorylation on αSyn-induced toxicity and trafficking defects in yeast, we generated strains that stably express WT αSyn-GFP or the phosphorylation mutants S129A-GFP or S129E-GFP from one or two genomic loci in the BY4741 strain background (Table 1). As expected, αSyn-GFP reduced cell growth in a dose-dependent manner (Fig. 4A). However, replacement of S129 by A or E did not alter αSyn-GFP toxicity or expression levels (Fig. 4A and B). These results suggest that phosphorylation at S129 does not modulate αSyn toxicity in the BY4741 strain background (although phosphorylation of other targets by Yck1 and Yck2 modulates αSyn toxicity as shown before). However, since the S129 phosphorylation status appears to govern αSyn neurotoxicity in fly and rat models (31,43), but not in two other models (29,32), we reasoned that variations in the genetic background of the models might account for the differential sensitivity of cells to the αSyn phosphorylation status.

To test this hypothesis, we generated strains that stably express WT αSyn-GFP or the phosphorylation mutants S129A-GFP or S129E-GFP from one or two genomic loci in the W303-1A genetic background (Table 1). This strain carries a mutation in the *YBP1* gene that increases its sensitivity to oxidative stress (44), a known mechanism of αSyn toxicity (45). Whereas one copy of any of the three αSyn-GFP alleles had no impact on yeast growth, two copies were detrimental in an allele-specific manner (Fig. 4C). Although the S129A mutation, which prevents phosphorylation, caused a dramatic increase in the growth defect caused by WT αSyn-GFP, the S129E-GFP mutation, which mimics phosphorylation, had no effect, suggesting that preventing phosphorylation enhances αSyn toxicity in the W303-1A strain background. Interestingly, the S129A-GFP mutation caused a significant ∼6-fold increase in the percentage of cells with αSyn-GFP inclusions in comparison with WT αSyn-GFP without altering expression levels (Fig. 4D–F), suggesting that blocking phosphorylation of S129 enhances trafficking defects caused by αSyn-GFP on the W303-1A genetic background.

To confirm this hypothesis, we studied the trafficking of the dye FM 4-64 in the strains with two copies of the WT αSyn-GFP gene, or the S129A-GFP and S129E-GFP mutations in the W303-1A background. As reported previously (33), WT αSyn-GFP impaired the delivery of the dye to the vacuolar membrane (Fig. 4G and H). The S129A-GFP mutation significantly enhanced this defect, indicating that the enhancement of toxicity correlates with increased trafficking defects. Importantly, these defects were typically observed only in cells with αSyn inclusions (Fig. 4I), regardless of the αSyn variant expressed, confirming that the formation of inclusions is an indication of underlying trafficking defects and suggesting a molecular link between phosphorylation and trafficking.

To verify whether the modulation of αSyn toxicity by Yck1 observed in the BY4741-derived strain is mediated by S129 phosphorylation or an independent mechanism, we deleted or overexpressed *YCK1* in strains expressing two copies of the WT αSyn-GFP gene, or the S129A-GFP and S129E-GFP mutations in the W303-1A background. Unexpectedly, either deletion or overexpression of *YCK1* did not alter the growth defect of these strains, whether expressing WT αSyn-GFP or the S129-GFP mutations (Fig. 4J). These observations demonstrate that the genetic modification of a toxic phenotype is profoundly influenced by the genetic background and may help explain paradoxical observations reported in different models of αSyn toxicity.

Evidence of endosome anomalies and CKIδ mislocalization in αSyn transgenic mice and in synucleinopathy brains

To determine whether defects in early-endocytic trafficking are a conserved pathologic feature of synucleinopathies, we studied the subcellular localization of the EE protein marker Rab5 in brain tissues from a transgenic (tg) mouse model of synucleinopathy (46) and human DLB/PD. In tg mice, overexpression of human αSyn results in the formation of αSyn-positive inclusion-like structures in the neocortex, hippocampus and substantia nigra (SN) by 2 months of age (46). In non-tg mice, Rab5 labeled discrete punctuate endosomes in the cytosol of cortical neurons at 6 months of age, whereas αSyn stained discrete puncta in the cell periphery. However, in tg animals, Rab5 labeled abnormally swollen endosomes in neurons that contained αSyn-positive intracellular inclusions (Fig. 5). Interestingly, the swollen endosomes co-localized with small granular aggregates of αSyn, but were excluded from large Lewy-body-like inclusions. Similarly, in cortical sections of human control subjects, Rab5 and αSyn exhibited a punctuate pattern that rarely co-localized. However, in human DLB/PD cases, Rab5 stained abnormal endosomal compartments that co-localized with αSyn granular aggregates but not with LBs. Although the nature of the enlarged Rab5-positive endosomes is unknown and they may not be equivalent to the accumulation of vesicles observed in yeast-overexpressing αSyn, the presence of these abnormal endosomes suggests that dysfunction of the endocytic pathway may occur in αSyn tg mice.

To examine the early-endocytic trafficking machinery in pathologic states *in vivo*, we analyzed by western blot the levels of Rab5 and two other EE markers, Rab4 and EEA1, in the αSyn tg mice and in a tg mouse model of Alzheimer's disease (AD), a non-strict form of synucleinopathy in which a processed fragment of αSyn deposits in extracellular amyloid plaques. In this model, expression of mutant human amyloid precursor protein (APP) leads to the formation of plaques in the frontal cortex by 4 months of age (47). At 6 months of age, both models exhibited elevated levels of monomeric and high molecular weight (HMW) species of αSyn in detergent-insoluble brain fractions (Fig. 6A and B). This change correlated with an apparent accumulation of Rab4 and HMW forms of Rab5, but no alterations in the mobility or levels of EEA1.

To validate these observations, we analyzed Rab5, Rab4 and EEA1 levels in two subgroups of human amyloidopathies,

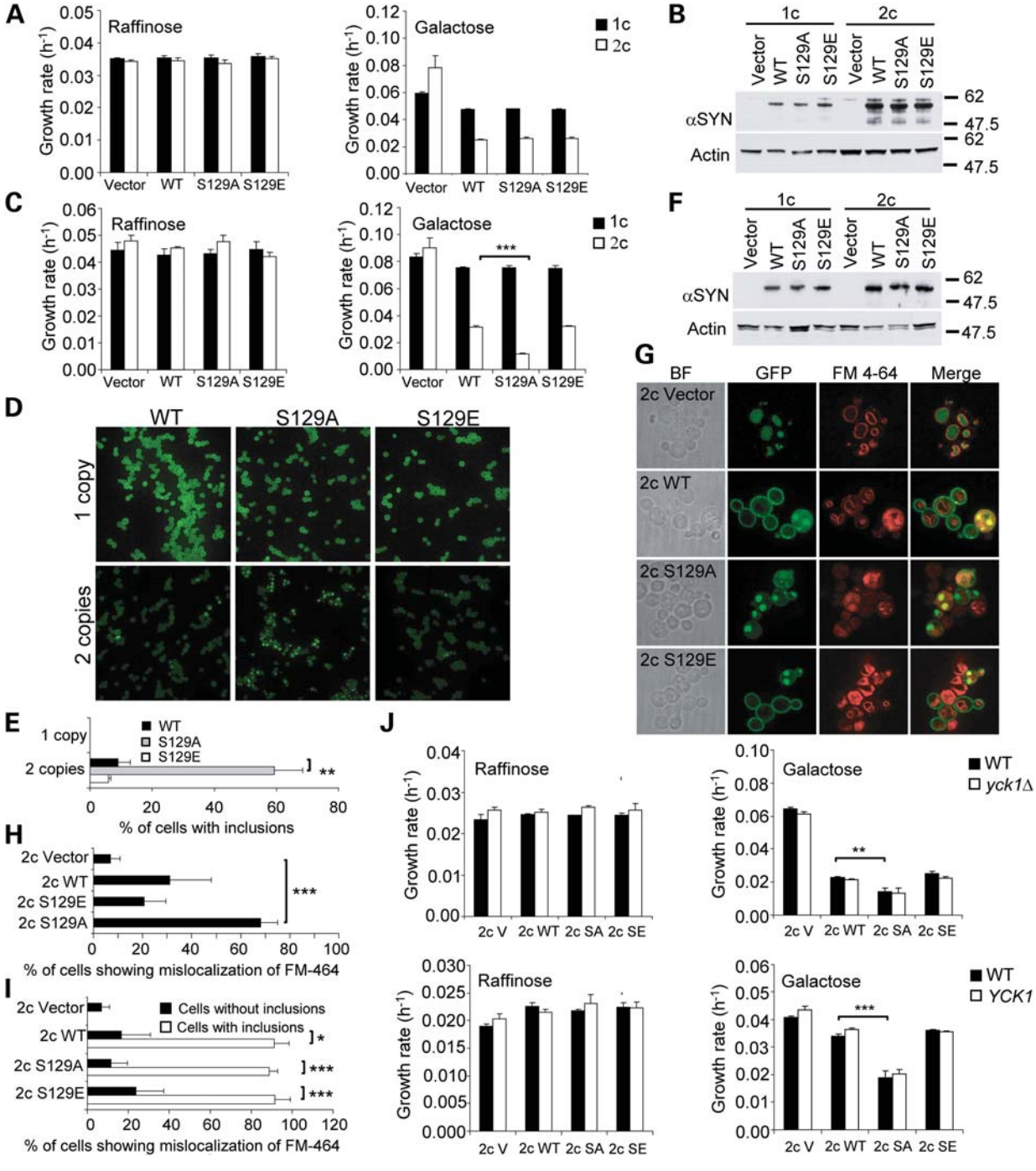

Figure 4. Preventing phosphorylation of S129 increases αSyn-induced toxicity and trafficking defects in a genetic context-dependent manner. (**A**) Growth rates of strains containing one (1c) or two (2c) copies of either the wild type (WT) αSyn-GFP gene or the phosphorylation mutants (S129A-GFP, S129E-GFP) or the corresponding empty vector in the BY4741 genetic background in conditions that do (galactose) or do not (raffinose) induce the expression of αSyn. (**B**) S129-GFP mutations do not alter the levels of αSyn in the BY4741 background. Western blot of strains from (A) grown for 8 h in galactose-containing medium. (**C**) Growth rates of strains containing one (1c) or two (2c) copies of either the WT αSyn-GFP gene or the phosphorylation mutants (S129A-GFP, S129E-GFP), or the corresponding empty vector in the W303-1A genetic background in conditions that do (galactose) or do not (raffinose) induce the expression of αSyn. (**D**) Localization of αSyn-GFP in the strains from (C) imaged in the logarithmic phase. (**E**) Quantification of the percentage of cells from (D) exhibiting αSyn inclusions. (**F**) S129 mutations do not alter the levels of αSyn-GFP in the W303-1A background. Western blot of strains from (C) grown for 8 h in galactose-containing medium. (**G**) Preventing S129 phosphorylation enhances mislocalization of FM 4-64 caused by αSyn-GFP in the W303-1A background. Strains from (C) were co-stained with the dye FM 4-64 and imaged in the logarithmic phase. (**H**) Quantification of the percentage of total cells from (G) showing mislocalization of the dye FM 4-64. (**I**) Quantification of the percentage of cells with and without inclusion from (G) showing mislocalization of FM 4-64. A high percentage of cells with inclusions display anomalies in the localization pattern of FM 4-64. (**J**) Deletion or overexpression of *YCK1* in the W303-1A background does not modify αSyn-induced growth defects. Growth rates of strains from (A) in which *YCK1* was either deleted (*yck1*Δ, upper panels) or overexpressed (*YCK1*, lower panels) in conditions that do (galactose) or do not (raffinose) induce the expression of αSyn-GFP. SA, S129A; SE, S129E. (C, E, H and I) Error bars represent standard deviations from three experiments. $^{*}P < 0.05$; $^{**}P < 0.01$; $^{***}P < 0.001$; (C, E, H, I and J) Student's *t*-test.

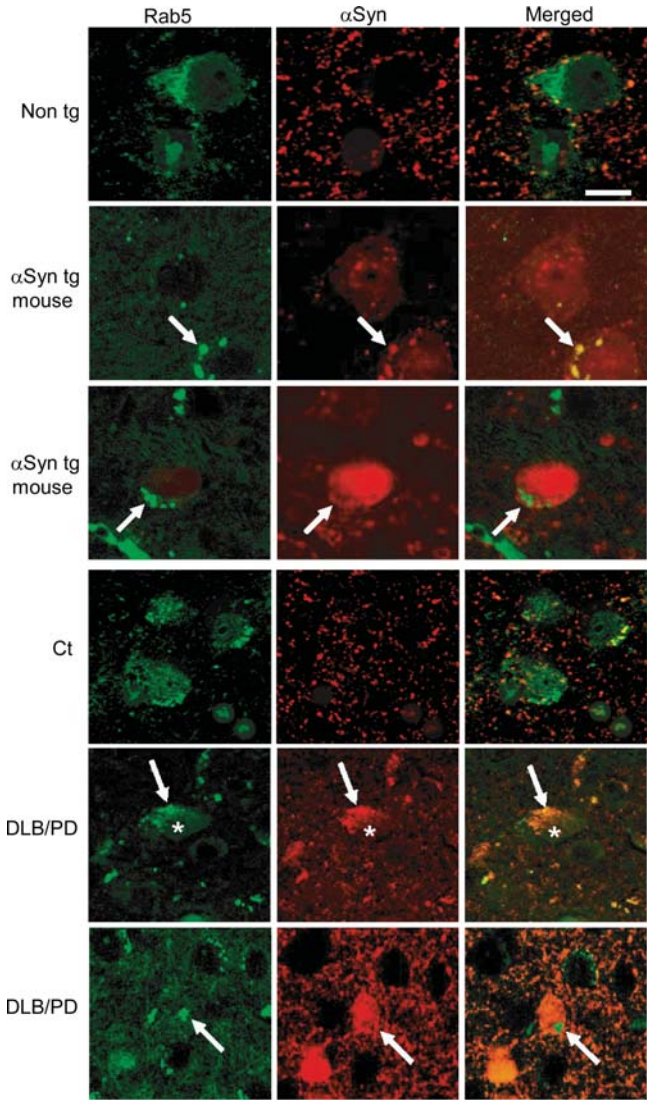

Figure 5. Abnormal endosome morphology in αSyn tg mice and in synucleinopathy brains. Abnormally enlarged Rab5-positive endosomes co-localize with granular inclusions of αSyn and accumulate in the vicinity of αSyn inclusions in αSyn tg mice and human DLB/PD. Cortical sections from αSyn tg mice or DLB/PD cases were double-labeled with antibodies against αSyn and Rab5 and detected with Tyramide Red or FITC-conjugated secondary antibodies, respectively. Images of non-tg animals and control (Ct) subjects are included for reference. Arrows indicate the Rab5-positive compartments. Scale bar, 10 μm.

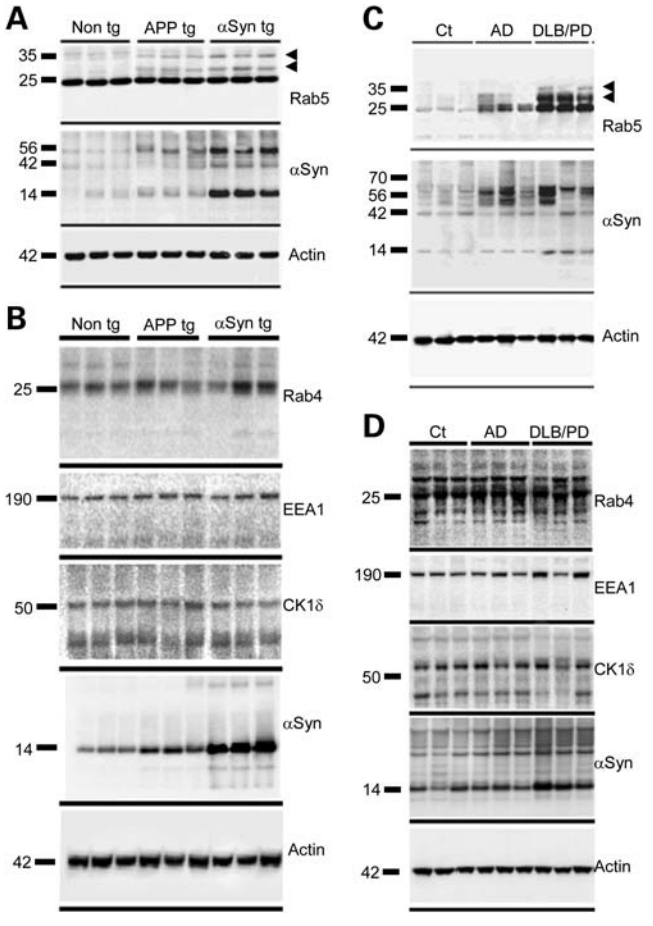

Figure 6. Analysis of levels of the EE markers Rab5, Rab4 and EEA1, and of mammalian CK1δ in mice models and human synucleinopathies. Brain particulate fractions from αSyn tg, APP tg or non-tg mice (**A** and **B**) or from human DLB/PD or AD patients or control (Ct) subjects (**C** and **D**) were analyzed by western blot with the indicated antibodies. Arrowheads indicate HMW forms of Rab5.

including DLB/PD and AD. Consistent with the mouse studies, detergent-insoluble HMW species of αSyn accumulated in strict synucleinopathies and AD cases compared with age-matched control subjects (Fig. 6C and D). In addition, levels of Rab5, but not Rab4 or EEA1, were markedly elevated in DLB/PD and AD relative to controls. As in the mice models, Rab5 exhibited a mobility shift to HMW forms in all the amyloidopathy cases studied, whereas the mobility of Rab4 or EEA1 was unchanged. Although the functional significance of the Rab5 mobility shift is unknown, the co-localization of αSyn granular aggregates with enlarged endosomes and the correlation between accumulation of αSyn HMW species and Rab5 suggest a causative role for αSyn in EE dysfunction. Consistent with this hypothesis, using small hairpin RNA-mediated gene knock down and overexpression studies, we recently found that stx7, Vps24, Vps28, Vps34, Vps45 and Vps52, proteins involved in endosomal transport, modulate αSyn toxicity in a dopaminergic SH-SY5Y neuroblastoma cell line and in primary neurons (Lee *et al*., manuscript in review).

To investigate a possible involvement of mammalian CKI proteins in the pathogenesis of synucleinopathies *in vivo*, we studied the subcellular localization of CKIδ, involved in vesicle transport (48,49), in brain sections from αSyn tg mice and human DLB/PD (Fig. 7). As expected, CKIδ localized predominantly to the cell periphery in cortical neurons from non-tg animals. In contrast, CKIδ co-localized with αSyn inclusions in tg animals. Importantly, this association was also found in neuronal inclusions in human DLB/PD, consistent with the notion that CKIδ may be sequestered by/recruited to αSyn inclusions in synucleinopathies.

Elevated levels of CK1δ mRNA have been detected in AD brains (50), suggesting that upregulation of CK1δ may be a

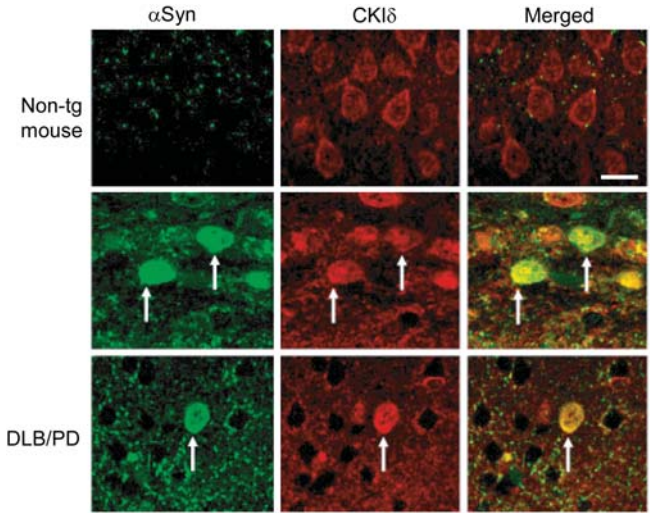

Figure 7. CKIδ co-localizes with αSyn inclusions in αSyn tg mice and human DLB/PD. Cortical sections from non-tg mice, αSyn tg mice or human DLB/PD cases were double-labeled with antibodies against αSyn and CKIδ and detected with FITC and Tyramid Red-conjugated secondary antibodies, respectively. Arrows indicate the αSyn-positive inclusions. Scale bar, 10 μm.

compensatory response in AD. To investigate whether CK1δ is upregulated in synucleinopathies, we analyzed the levels of CK1δ by western blot in brains from αSyn and APP tg mice and human DLB/PD and AD cases (Fig. 6B and D). We did not detect any significant changes in the levels of CK1δ in mice models or human synucleinopathies, indicating that CK1δ is not upregulated in response to αSyn accumulation. CKIδ levels were also apparently unchanged in AD cases, suggesting that the observed mRNA upregulation in AD may not lead to increased CK1δ synthesis, or that the upregulation is tissue-specific and undetectable in whole-brain homogenates.

DISCUSSION

A number of recent studies have shown that αSyn overexpression causes vesicle trafficking defects in a wide variety of model systems (7–10,12,13,15,17) by perturbing SNARE function (11,51,52). In yeast, an early effect of expressing αSyn by a strong galactose-inducible system is an ER-to-Golgi block that precedes a global trafficking failure (12,13). This trafficking collapse is accompanied by the formation of αSyn-positive vesicular clusters that co-localize with protein markers of several trafficking routes, including ER-to-Golgi, intra-Golgi, Golgi-to-PM, EE-to-LE, and LE-to-vacuole (13,15). The presence of endosome-to-Golgi markers in the clusters is controversial since Gitler *et al*. (13) detected Ypt6, but Soper *et al*. (15) failed to detect Vps17 or Vps29. Importantly, the Rab GTPase Ypt1 and the SNARE Ykt6, involved in ER-to-Golgi vesicle-mediated transport, suppress αSyn-induced trafficking defects (11–13).

In this study, we present evidence of the steady-state impairment of late-exocytic, early-endocytic and/or recycling trafficking by constitutive expression of αSyn in yeast from the *GPD1* promoter. In agreement with previous studies, we observed that trafficking defects coincide with an accumulation of αSyn-positive vesicles that originate in the vicinity of the cell surface and progressively expand toward the cell interior. The vesicles co-label with Snc1, an exocytic SNARE that is targeted to the PM and subsequently internalized and recycled for re-use via EE and the Golgi, implying that at least some of the vesicles originate in the Golgi or the PM. We propose that, in our system, αSyn blocks a trafficking step that follows vesicle budding from the Golgi or the PM and precedes fusion to target membranes. However, we cannot exclude the possibility that the observed vesicles constitute a cellular response to cope with the αSyn overload by compartmentalizing the toxic protein.

In our studies, αSyn did not impair the targeting of a number of protein trafficking markers traversing the ER and the Golgi toward the vacuole, indicating that ER-to-Golgi transport is unaffected in our model. The discrepancy between our findings and previous studies may be reconciled by differences in the expression levels, toxicity and duration of the insult attained by distinct expression systems (53,54). Whereas prior studies used a galactose-inducible promoter, our studies used a constitutive promoter to assess the effects of αSyn expression on protein trafficking. Interestingly, in the current study, we show that Ypt1 rescues the mislocalization of GFP-Snc1-Sso1 caused by constitutive αSyn expression. Although it is well established that Ypt1 functions in ER-to-Golgi trafficking, this protein also facilitates the recycling of internalized PM proteins (55). Therefore, we propose that Ypt1 rescues αSyn toxicity by promoting, at least in part, the recycling of PM proteins. Consistent with this interpretation, Ypt6, which is involved in endosome-to-Golgi and intra-Golgi retrograde transport (56), was also shown to partially suppress αSyn toxicity (12,13). Thus, although it is conceivable that the trafficking defects that we observed might be secondary to the sustained imposition of the primary ER-to-Golgi block, in our system, αSyn appears to directly impair late-exocytic, early-endocytic and/or recycling trafficking without affecting other pathways.

Our observations contribute to accumulating evidence that trafficking defects are a conserved mechanism of pathogenesis in human synucleinopathies. In yeast, Rab GTPases governing multiple trafficking steps are sequestered by αSyn-induced vesicle clusters (13). Similarly, in humans, members of the Rab family implicated in exocytosis (Rab3a), endocytosis (Rab5) and polarized traffic (Rab8a) interact aberrantly with αSyn in DLB and co-localize with αSyn glial inclusions in MSA (57–59). Conversely, Rab1 (involved in ER-to-Golgi transport), Rab3a and Rab8a are neuroprotective in cellular and animal models in which αSyn is overexpressed (12,13). In catecholaminergic cells, αSyn impairs exocytosis, leading to an accumulation of docked vesicles (9). Finally, clusters of dense core vesicles have been observed in the perimeter of LBs (15,60,61).

Our study provides evidence of anomalies in endosome morphology and the endocytic Rab5 in pathologic states *in vivo*. In mouse models and human synucleinopathies, EE are abnormally enlarged in cortical neurons and Rab5 co-localizes with αSyn granular inclusions and accumulates abnormally in detergent-insoluble fractions from brain lysates. Similarly, we observed an increase in the levels of Rab4 in αSyn tg mice, but

not in human DLB/PD cases, whereas the levels of EEA1 were unchanged in mice and humans. Both Rab4 and Rab5 are GTPases involved in early endocytic trafficking, although they differ in their functional specialization. Whereas Rab5 regulates the fusion between endocytic vesicles and EE, as well as the homotypic fusion between EE (62), Rab4 controls the function or formation of endosomes involved in endocytic recycling (63). In contrast, EEA1 is a Rab5 effector (64). Therefore, αSyn appears to alter the function of endocytic Rab GTPases without altering the levels of downstream effectors. In agreement with our observations, inhibition of Rab5 GTPase activity results in the formation of unusually large early endocytic structures (65), a phenotype mimicked by the overexpression of αSyn. These alterations suggest that endocytic trafficking defects might also occur and contribute to neuronal dysfunction in synucleinopathies. In striking similarity to our yeast studies, an RNAi screen in the nematode *C. elegans* showed that endocytosis-defective mutants potently exacerbate αSyn neurotoxicity (17). Worms that overexpressed αSyn displayed decreased neurotransmitter release, similar to endocytosis-defective mutants. These authors also reported that the knock down of a CK1 gene enhances αSyn toxicity, and showed that αSyn phosphorylated at S129 accumulated in mutants defective in endocytosis (17).

In agreement with this model, we found that deletion of *YCK1* or *YCK2*, two redundant kinases of the CKI family that promote the endocytosis and delivery of PM proteins to the vacuole, led to an increase in αSyn toxicity. Interestingly, *yck1*Δ cells accumulate cargo normally destined for the vacuole in an endocytic compartment, but do not affect trafficking through the CPY and ALP pathways to the vacuole (37). These results are further supported by our previous studies in which the yeast SNARE Tlg2 was identified as a loss-of-function enhancer of αSyn toxicity (20). Tlg2 participates in endosome-to-Golgi recycling and is required for targeting Yck2 to the PM (39), suggesting that exacerbation of αSyn toxicity in *tlg2*Δ cells might be due, at least in part, to decreased CKI activity at the PM. Although we did not detect any significant increase in trafficking defects upon deletion of *YCK1*, we observed a reduction in αSyn-induced growth and trafficking defects upon overexpression of *YCK1*. Although Yck1 contributes modestly to the phosphorylation of αSyn at S129, our results indicate that the attenuation of the toxicity and trafficking defects is not mediated by increased phosphorylation of αSyn. Thus, it is conceivable that CKI activity protects against αSyn toxicity by directly promoting PM endocytosis. This hypothesis is consistent with the observation that knocking down the *C. elegans YCK1* ortholog *csnk-1* by RNAi causes synaptic deficits selectively in αSyn tg worms (17).

The function of S129 phosphorylation in physiologic and pathologic conditions is unclear. Although only a small fraction of αSyn is phosphorylated in the healthy brain, αSyn is hyperphosphorylated at S129 in pathologic lesions (21,22,66). However, the relevance of S129 phosphorylation to disease pathogenesis is unknown since conflicting observations have been reported. Mimicking phosphorylation has been shown to be neuroprotective (31) or innocuous (29,32) in rats, but detrimental in *Drosophila* (30), and SH-SY5Y and oligodendroglial cells (41,42). We showed that, in yeast, the effect of S129 phosphorylation on αSyn toxicity is exquisitely dependent on genetic context; although blocking S129 phosphorylation is innocuous in BY4741-derived yeast strains, this markedly increased the toxicity and trafficking defects caused by αSyn in W303-1A-derived strains, supporting a protective role for phosphorylation in specific genetic contexts. Interestingly, W303-1A carries a mutation in the *YBP1* gene that decreases oxidative stress responses and increases the sensitivity to oxidative stress. This genetic variability could contribute to the differential sensitivity between the two strain backgrounds to S129A αSyn. Consistent with this hypothesis, αSyn causes oxidative stress and ROS accumulation and increases the vulnerability of yeast to hydrogen peroxide (16,67). Conversely, antioxidants and genes involved in the stress response suppress αSyn toxicity in yeast (18,68).

Taken together, our studies indicate that αSyn toxicity is linked to trafficking defects and that this phenotype is modulated by phosphorylation-dependent and -independent pathways. For example, the attenuation of toxicity and trafficking defects by *YCK1* appears to be uncoupled from S129 phosphorylation. However, the relative contribution of each pathway to αSyn toxicity appears to be dependent on the genetic landscape of the cell.

A previous study by Zabrocki *et al*. (14) showed that Yck1, Yck2, Yck3 and CKII phosphorylate αSyn at S129. However, although deletion of *YCK1* and *YCK2* modestly alleviated an αSyn-induced growth defect and stabilized αSyn at the PM, deletion of *YCK3* and the four subunits of CKII (*CKA1*, *CKA2*, *CKB1* and *CKB2*) exacerbated the growth defect and resulted in αSyn accumulation in intracellular compartments. The latter observation is consistent with the genetic context-dependent enhancement of αSyn toxicity and inclusion formation by the S129A allele we report in this study. Therefore, despite some discrepancies regarding the effects of CKs on αSyn toxicity, the general conclusion arising from both studies is that impairment of endocytic trafficking can at least partially account for increased αSyn toxicity.

There is substantial evidence that mammalian CKs phosphorylate αSyn at S129 in cultured cells and *in vivo* (22–24). In neurons, a number of mammalian CKI isoforms associate with synaptic vesicles, and the phosphorylation of CKI substrates is thought to regulate synaptic vesicle trafficking and neurotransmission. Mammalian CK substrates include proteins implicated in synaptic vesicle formation (AP-3 adaptor complex) (69), docking and fusion (p65) (70) and exocytosis (synaptotagmin I) (71), and in the storage of neurotransmitters (VMAT2) (72). Interestingly, some CKI mRNA isoforms (α, δ and ε, but especially δ) are dramatically upregulated in the hippocampus and associated with tau-containing neurofibrillary tangles in AD and other dementias (50). Here, we describe for the first time the co-localization of CKIδ with LBs in DLB/PD, suggesting that CKIδ may be sequestered in a manner that might prevent proper phosphorylation of its canonical substrates in synucleinopathies.

Based on our observations and previous studies, we have generated a model to describe the cascade of pathogenic events that lead to neuronal dysfunction and death in synucleinopathies (Fig. 8). As αSyn is normally a synaptic vesicle-associated protein, we hypothesize that, under physiologic conditions, CKIδ regulates neurotransmission by

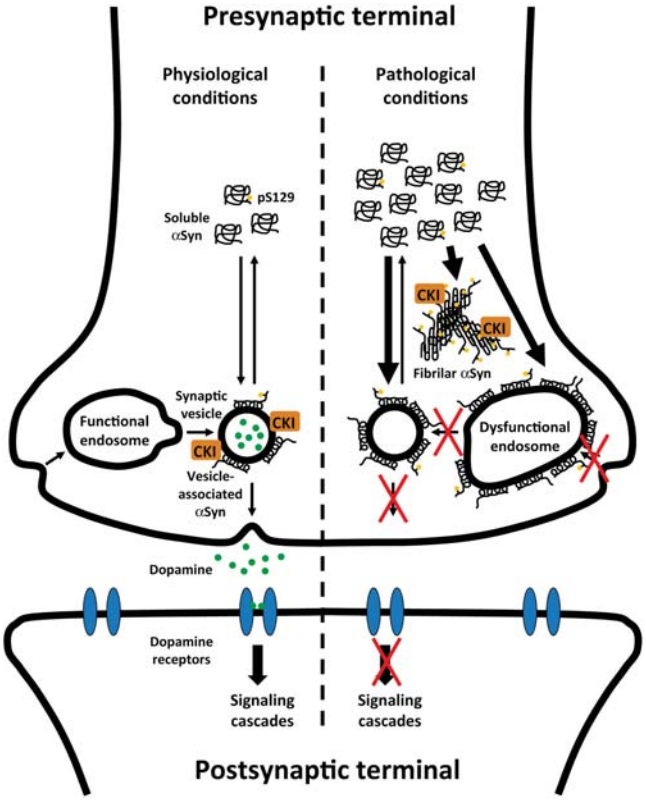

Figure 8. A model depicting how αSyn accumulation may cause neurotransmission defects in PD. We hypothesize that, under normal conditions, CKI regulates αSyn function and, possibly, association with synaptic vesicles and neurotransmitter release by phosphorylating synaptic proteins, including αSyn at S129. Under pathologic conditions in which αSyn accumulates and synaptic trafficking and neurotransmission are compromised, CKI may play a protective role in attenuating vesicular trafficking defects and restoring synaptic transmission. However, when all binding sites in synaptic vesicles are saturated, excess αSyn may associate with other compartments, such as endosomes, leading to abnormally enlarged endosomes and defects in synaptic vesicle homeostasis and neurotransmission. In addition, excess αSyn may form insoluble fibrillar deposits that sequester CKI, depleting CKI activity and enhancing synaptic defects. Red crosses indicate possible trafficking steps blocked by αSyn.

phosphorylating synaptic proteins, potentially including αSyn. Under pathologic conditions, the progressive accumulation of αSyn may lead to sequestration of Rab GTPases and deficits in vesicular endocytic/exocytic/recycling trafficking that ultimately impair neurotransmitter release. We speculate that when all binding sites in synaptic vesicles are saturated, excess αSyn may associate with other compartments, including endosomes, leading to sustained defects in synaptic vesicle homeostasis and neurotransmission. CKIδ-dependent phosphorylation of vesicular substrates, including αSyn, may play a protective role by attenuating trafficking defects and stabilizing synaptic transmission. In addition, excess αSyn deposited in LBs may irreversibly sequester CKIδ and other vesicle-associated proteins, resulting in the loss of CKIδ activity and reduced protection against these defects. In summary, our study provides additional evidence that vesicular trafficking defects involving endocytosis and exocytosis and CKIδ dysfunction may be relevant for the pathogenesis of synucleinopathies.

MATERIALS AND METHODS

Plasmids

Plasmids p426GPDαSyn(WT)GFP, p426GALαSyn(WT)GFP, pGS416 (*GFP-SNC1*), pGSSO416 (*GFP-SNC1-SSO1*), pGNS416 (*GFP-NYV1-SSO1*), pPEP416 (*GFP-PEP12*), pPHM5 (*GFP-PHM5*) and pSNA3416 (*SNA3-GFP*) have been described (33–36).

Plasmid pSTE2416 was created by replacing the *SNA3* gene from plasmid pSNA3416 (36) with the *STE2* gene as a *Hin*dIII–*Age*I-digested product of PCR amplification.

Plasmid p8xmycSNC1416 (8x*MYC-SNC1*) was created by replacing the *GFP* gene from plasmid pGS416 with the 8x*MYC* sequence as a *Hin*dIII–*Eco*RI-digested product of PCR amplification. Plasmid p8xmycSNC1406 was then created by subcloning the *TPI1pr-8xMYC-SNC1* fusion from plasmid p8xmycSNC1416 into the *Xho*I and *Bam*HI sites of the pRS406 integrating vector (73). p8xmycSNC1406 was linearized with *Eco*RV for integration.

Plasmid pmCheSSO416 (*mCherry-SNC1-SSO1*) was created by replacing the GFP tag from plasmid pGSSO416 with the mCherry gene from plasmid pmCheV5ATG8406 (74) as an *Xho*I–*Eco*RI fragment. Plasmid pmCheSSO415 was created by subcloning the *TPI1pr-mCherry-SNC1-SSO1* fusion from plasmid pmCheSSO416 into the *Xho*I and *Sac*I sites of the plasmid p415TEF (54).

Plasmid p423GPDαSYN(WT)GFP was created by subcloning the *SNCA*(WT)-*GFP* fusion from plasmid p426GALα SYN(WT)GFP into the *Spe*I and *Xho*I sites of plasmid p423GPD (54).

Plasmid p423GPDαSYN(WT) was created by subcloning *SNCA*(WT) from plasmid p426GPDαSYN(WT)GFP into the *Sac*I and *Xho*I sites of p423GPD (54).

Plasmids p426GALαSYN(S129A)GFP and p426GALα Syn(S129E)GFP were created by recombining PCR-amplified *SNCA*(S129A) and *SNCA*(S129A) (kindly provided by Dr Robert Edwards, UCSF) into *Bam*HI-linearized p426GALα SYN(WT)GFP. Plasmids pRS304αSYN(WT)GFP, pRS304α SYN(S129A)GFP, pRS304αSYN(S129E)GFP, pRS306αSYN (WT)GFP, pRS306αSYN(S129A)GFP, pRS306αSYN (S129E)GFP were then created by subcloning the *GAL1pr-SNCA*(WT, S129A and S129E)-*GFP* fusions from the p426GAL-derived plasmids into the *Sac*I and *Kpn*I sites of the integrating vectors pRS304 and pRS306 (73). Plasmids pRS304(MCS-) and pRS306(MCS-), lacking the multiple cloning site, were created by digesting pRS304 and pRS306 with *Sac*I and *Kpn*I, blunting the ends with DNA Polymerase I, Large (Klenow) Fragment (New England Biolabs) and re-circularizing the plasmids. pRS304- and pRS306-derived plasmids were linearized with *Eco*RV for integration into the W303-1A strain.

Plasmids pRS405TRP1αSYN(WT)GFP, pRS405TRP1αSYN (S129A)GFP and pRS405TRP1αSYN(S129E)GFP were generated by sequential insertion of the *GAL1pr-SNCA*(WT, S129A and S129E)-*GFP* fusions from the p426GAL-derived plasmids into the *Sac*I and *Kpn*I sites of the integrating vector pRS405, followed by insertion of the first and the last 300 bp of the *TRP1* ORF in inverted order (3′5′) separated by an *Xma*I site into the *Sac*I site of plasmid pRS405 for gamma integration into the *TRP1* locus. Plasmid

pRS405TRP13′5′ was generated by removing the *GAL1pr-SNCA*(WT, S129A and S129E)-*GFP* insert within the *Spe*I and *Xho*I sites, blunting the ends with DNA Polymerase I, Large (Klenow) Fragment (New England Biolabs) and re-circularizing the plasmids.

Plasmids pRS406PDR1αSYN(WT)GFP, pRS406PDR1α SYN(S129A)GFP and pRS406PDR1αSYN(S129E)GFP were generated by sequential insertion of the *GAL1pr-SNCA*(WT, S129A and S129E)-*GFP* fusions from the p426GAL-derived plasmids into the *Sac*I and *Kpn*I sites of the integrating vector pRS406, followed by insertion of the first and the last 300 bp of the *PDR1* ORF in inverted order (3′5′) separated by an *Mfe*I site into the *Sac*I site of plasmid pRS406 for gamma integration into the *PDR1* locus. Plasmid pRS406PDR13′5′ was generated by removing the *GAL1pr-SNCA*(WT, S129A and S129E)-*GFP* insert within the *Age*I and *Xho*I sites, blunting the ends with DNA Polymerase I, Large (Klenow) Fragment (New England Biolabs) and re-circularizing the plasmids.

pRS405- and pRS406-derived plasmids were linearized with *Xma*I and *Mfe*I, respectively, for integration into the Y5563 strain.

Plasmids p425GALYPT1 and p425GALYCK1 were created by subcloning *YPT1* and *YCK1* from the Yeast ORF collection (Open Biosystems) into p425GAL (53) (Addgene), using Gateway Technology (Invitrogen).

Plasmid p415YCK1 was created by cloning *YCK1* with its endogenous promoter into plasmid p415TEF (54) as a *Sac*I–*Bam*HI-digested product of PCR amplification from yeast genomic DNA.

Yeast strains and manipulation

The strains used in this study are summarized in Table 1.

To generate strain VSY1, the *GAL1pr-SNCA*(WT)-*GFP* fusion was PCR-amplified from plasmid p426GALα SYN(WT)GFP, and the *MX4-NatR* cassette was PCR-amplified from plasmid p4339 (kindly provided by Dr Charles Boone, University of Toronto). Primer sequences were designed to enable the merging of both fragments in a third PCR reaction and the site-directed integration of the resulting *GAL1pr-SNCA*(WT)-*GFP-NatR* fusion at the *ADE2* locus by homologous recombination in the BY4741 strain (75).

To generate strain VSY2, the *GAL1pr-SNCA*(WT)-*GFP* fusion was PCR-amplified from plasmid p426GALα SYN(WT)GFP, and the *URA3-MX6* cassette was PCR-amplified from plasmid p4348 (kindly provided by Dr Charles Boone, University of Toronto). Primer sequences were designed to enable the merging of both fragments in a third PCR reaction and the site-directed integration of the resulting *GAL1pr-SNCA*(WT)-*GFP-URA3* fusion at the *TRP1* locus by homologous recombination in the Y5563 strain (76).

To generate strain VSY4, strains VSY1 and VSY2 were crossed. Diploid cells were selected on SD−Ura + G418 (Invitrogen)/ClonNAT (Werner BioAgents) plates and sporulated. Spores were germinated and haploid cells of both mating types were selected in SD−Arg/Lys/Ura + canavanine (Sigma-Aldrich)/thialysine (Sigma-Aldrich)/G418/clonNAT plates. *MAT*α cells were selected by their inability to grow on SD−His plates, and the mating type was subsequently confirmed by mating test.

Strains VSY53-61 were obtained from a cross between strain VSY4 and the corresponding deletion strains.

Strains *pdr1*Δ, *yck1*Δ, *yck2*Δ, *tlg2*Δ and *spo14*Δ were retrieved from the Yeast *MAT***a** Genome Deletion Collection (Open Biosystems).

Strain VSY5 was generated by disruption of the *PDR1* gene from strain VSY4 with the *kanMX4* cassette obtained by PCR amplification of genomic DNA from strain *pdr1*Δ.

Strain VSY24 was generated by disruption of the *kanMX4* cassette from strain VSY17 with the *LEU2* cassette obtained by PCR amplification from plasmid pRS415.

Strain VSY25 was generated by disruption of the *PDR1* gene from strain VSY24 with the *kanMX4* cassette obtained by PCR amplification of genomic DNA from strain *pdr1*Δ.

Strain FRY346 was generated by integration of *Eco*RV-linearized p8xmycSNC1406 plasmid in the BY4741 strain.

Strains VSY67 to VSY74 were generated by consecutive integration of *Eco*RV-linearized pRS306- and pRS304-derived plasmids in the W303-1A strain.

Strains VSY75-78 were generated by disruption of the *YCK1* gene from strains VSY71-78 with the *kanMX4* cassette obtained by PCR amplification of genomic DNA from strain *yck1*Δ.

Strains VSY79-86 were generated by consecutive integration of *Xma*I-linearized pRS405-derived plasmids, followed by integration of *Mfe*I-linearized, pRS406-derived plasmids in the Y5563 strain.

Strains BY4741 and FRY346 were transformed with the indicated plasmids, using the one-step protocol (43) and cultured in synthetic complete medium without the corresponding nutrients for auxotrophic selection and with the indicated carbon sources.

The integrated strains were transformed using the standard protocol (77) and cultured in rich (YEP) medium with the indicated carbon sources.

Yeast growth curves

The indicated strains were inoculated in triplicate in 100 μl of raffinose-containing medium in 96-well plates and grown for 48 h to the stationary phase. Cultures were then diluted 100-fold in raffinose- and galactose-containing media and incubated at 30°C. The OD_{600} was recorded at the indicated times. Growth rates were determined as the slope of the growth curves during the logarithmic phase.

Pharmacologic inhibition of CKI activity

For the CKI inhibitor studies, strains *pdr1*Δ (0c αSyn in *pdr1*Δ), VSY5 (2c αSyn in *pdr1*Δ) and VSY24 (2c αSyn in *pdr1*Δ *yck1*Δ) were grown in raffinose-containing medium to the stationary phase, diluted to $OD_{600} = 0.1$ in raffinose- and galactose-containing media and dispensed in 100 μl of aliquots to 96-well plates. Aliquots were treated in triplicate with the indicated concentrations of D4476 (Calbiochem, CA, USA) or vehicle DMSO alone.

Table 2. Characteristics of human cases analyzed in this study

Group	Age (years)	Gender M/F[a]	Blessed score (range)	Braak stage (range)	Plaques per mm^2	Tangles per 0.1 mm^2	Lewy bodies	Brain weight (g)
Non-demented ($n = 4$)	83 ± 2	2/2	0–1	0–1	0.25	0	0	1150 ± 40
AD ($n = 6$)	81 ± 2	3/3	13–33	5–6	25 ± 3	5 ± 1	0	1070 ± 35
DLB/PD ($n = 8$)	83 ± 1	5/3	6–33	2–4	28 ± 3	2 ± 1	3 ± 1	1110 ± 60

[a]Males/Females.

Phosphorylation assays

For the time-course experiment, strain VSY4 (2c αSyn in WT) was grown to the logarithmic phase ($OD_{600} \approx 0.8$) in raffinose-containing medium, and αSyn expression was induced by adding 0.2% galactose. At the indicated times, 8 ml of aliquots were collected. For protein extraction, cells were collected by centrifugation, washed with water and resuspended in 200 µl of extraction buffer [200 mM Tris, pH 8.0, 150 mM ammonium sulfate, 10% glycerol, 1 mM EDTA, 1 µM microcystin LR, 200 µM activated Na_3VO_4 and 1 × complete protease inhibitor cocktail (Roche)] and 100 µl of acid-washed glass beads (425–600 µm) (Sigma-Aldrich). Cells were lysed by vortexing two times for 5 min at 4°C. Supernatants were separated from cell debris and beads by centrifugation at 5000 r.p.m. for 5 min and then cleared by centrifugation at 13 000 r.p.m. for 30 min. The soluble fractions (supernatant) were separated by SDS–PAGE and proteins analyzed by immunoblot with mouse anti-αSyn (1:20 000) (BD Transduction Laboratories) and anti-S129 phospho-specific antibodies (1:20 000) (JH22.11A5, Elan Pharmaceuticals).

For comparison of αSyn phosphorylation levels in different deletion backgrounds, strains VSY4, VSY17, VSY58 and VSY60 were grown to the logarithmic phase ($OD_{600} \approx 0.8$) in raffinose-containing medium, and αSyn expression was induced by adding 0.2% galactose for 1 h. Samples were treated as described before, and soluble fractions were analyzed by western blot. Band densities were quantified with ImageQuant 5.2 (Molecular Dynamics).

To assess αSyn phosphorylation in *YCK1*-overexpressing cells, the indicated strains were grown for 12 h to the logarithmic phase in raffinose-containing medium and induced with 2% galactose. At 5.5 and 11 h, 10 ml of aliquots were collected. When indicated, cultures were treated with 500 nM microcystin and 200 µM cell-permeable Na_3VO_4 for 15 min prior to cell harvesting. Samples were analyzed as described before.

Analysis of αSyn levels in yeast

Strains VSY67-74 and VSY79-86 were grown to the logarithmic phase in raffinose-containing medium and induced with 2% galactose for 8 h. Samples were processed and analyzed by western immunoblot as described before.

Analysis of αSyn, Rab5, Rab4, EEA1 and CK1δ cellular levels

Brain homogenates were solubilized in lysis buffer (1% Triton X-100, 10% glycerol, 50 mM HEPES, pH 7.4, 140 mM NaCl, 1 mM EDTA, 1 mM Na_3VO_4, 20 mM β-glycerophosphate and proteinase inhibitor cocktails) and separated into cytosolic and particulate fractions by centrifugation. Twenty milligrams of the particulate fractions were resolved by SDS–PAGE and blotted onto membranes before be decorated with rabbit polyclonal anti-αSyn (Chemicon), mouse monoclonal anti-Rab5 (BD Transduction Laboratories), mouse anti-human EEA1 (BD Transduction Laboratories), mouse anti-human Rab4 (BD Transduction Laboratories), goat anti-CK1δ (C-18) (Santa Cruz Biotechnology) and mouse monoclonal anti-actin (Chemicon).

Mouse models

For this study, 12 heterozygous tg, 6-month-old mice expressing human αSyn under the regulatory control of the platelet-derived growth factor-β promoter (Line D) (46) and 12 littermate non-tg, age-matched controls were used. These animals were selected because they display abnormal accumulation of detergent-insoluble αSyn, develop cytoplasmic αSyn-immunoreactive inclusion-like structures in the brain and display neurodegenerative and motor deficits that mimic certain aspects of DLB/PD (46,78–80). Comparisons of the patterns of αSyn and Rab5 distribution were performed with six tg 6-month-old mice that mimic AD-like pathology by expressing the human mutant APP (line 41) under the thy1 promoter (47).

Human cases and neuropathologic evaluation

This study examined a total of 18 subjects (Table 2), including 8 cases of DLB/PD, 6 cases of Alzheimer's disease (AD) and 4 non-demented controls. Autopsy material was obtained from patients studied neurologically and psychometrically at the Alzheimer Disease Research Center/University of California, San Diego (ADRC/UCSD). For each case, paraffin sections from 10% buffered formalin-fixed neocortical, limbic system and sub-cortical material stained with hematoxylin and eosin (H&E) and thioflavin-S were used for routine neuropathologic analysis (81,82) that included the Braak stage (83). The diagnosis of DLB/PD was based on the clinical presentation of dementia, followed by parkinsonism and the pathologic findings of LBs in the locus coeruleus, SN or nucleus basalis of Meynert, as well as in cortical and subcortical regions. LBs were detected using H&E anti-ubiquitin and anti αSyn antibodies as recommended by the Consortium on DLB criteria for a pathologic diagnosis of DLB/PD (84). In addition to the presence of LBs, the great majority of these cases

display sufficient plaques and tangles to be classified as Braak stages III–IV. Specifically, DLB/PD cases had abundant plaques in the neocortex and limbic system but fewer tangles compared with AD cases.

Fluorescence microscopy of yeast

For the S129 mutagenesis study, strains VSY67-74 were grown to the stationary phase at 30°C in raffinose-containing medium and diluted 100-fold in galactose-containing medium. Cells were induced for 16 h, mounted and sealed as described.

For the trafficking studies, strain BY4741 co-transformed with plasmids p423GPDαSYN(WT) or p423GPF and pGS416 (*GFP-SNC1*), pGSSO416 (*GFP-SNC1-SSO1*), pGNS416 (*GFP-NYV1-SSO1*), pPEP416 (*GFP-PEP12*), pPHM5 (*GFP-PHM5*), pSNA3416 (*SNA3-GFP*) or pSTE2416 (*GFP-STE2*) was grown for 12 h to the logarithmic phase at 30°C in glucose-containing medium and mounted as described. Strains BY4741, *yck1*Δ, VSY4 and VSY17 transformed with plasmid pmCheSSO416 (*mCherry-SNC1-SSO1*) were grown for 12 h to the logarithmic phase at 30°C in galactose-containing medium and mounted as described.

For FM 4-64 labeling, the indicated strains were grown for 12 h in medium containing glucose [deletion and temperature-sensitive mutant strains transformed with plasmid pGSSO416 (*GFP-SNC1-SSO1*)] or galactose (strains VSY71-74) at 30°C (deletion strains and VSY71-74) or RT (temperature-sensitive strains). A total of 0.16 culture ODs were centrifuged and resuspended in 40 μl of medium containing 40 μM FM 4-64 to a final OD_{600} of 4.0. Cells were pulsed with the dye for 15 min, washed with 1 ml of H_2O, resuspended in 0.5 ml of unlabeled medium and incubated for 1 h to let the dye internalize. The deletion and VSY71-74 strains were labeled at 30°C, whereas the temperature-sensitive strains were pre-incubated at 37°C or RT for 30 min prior to the FM 4-64 pulse and kept at the same temperature throughout all the steps for imaging.

For the rescue studies, strain BY4741 co-transformed with plasmids p423GPDαSYN(WT) or p423GPF alone, and pGSSO416 (*GFP-SNC1-SSO1*), was transformed with plasmids p425GALYPT1, p425GALYCK1 or left untransformed (no plasmid). Cells were grown in glucose-containing medium at 30°C to the stationary phase and diluted down 20-fold in galactose-containing medium. Cultures were induced for 16 h and prepared for imaging as described.

For the mutagenesis, trafficking, rescue and FM 4-64 studies, cells were imaged with a Nikon Plan Apo VC 100× (N.A. 1.4) objective on a spinning disc confocal microscope (Nikon) and images were acquired with a Cascade II digital camera (Photometrics), using Micro-Manager 1.3 (University of California, San Francisco).

IEM of yeast

For single-labeling, strain BY4741 transformed with the plasmid p426GALαSyn(WT)GFP was grown at 30°C in glucose-containing medium to the early logarithmic phase, washed with water, resuspended in galactose-containing medium and incubated for 6 or 12 h. For double-labeling, strain FRY346 transformed with plasmid p423GPDα SYN(WT)GFP was grown for 12 h at 30°C in glucose-containing medium to the logarithmic phase. In both cases, cells were fixed with 2% glutaraldehyde–0.2% para-formaldehyde and prepared for the Tokuyasu cryosectioning procedure according to a protocol optimized for *Saccharomyces cerevisiae* (85). Ultrathin sections were incubated first with antibodies recognizing the tags and subsequently with protein A-gold conjugates (86). After standard staining with uranyl and embedding in methylcellulose, sections were visualized in a JEOL 1010 electron microscope, and images were recorded on Kodak 4489 sheet films.

For single-labeling, a polyclonal anti-GFP antiserum was used (Abcam). For double-labeling, a monoclonal anti-myc antibody (Santa Cruz Biotechnology) and the same anti-GFP antiserum were used. Untransformed cells were treated in the same way and used as background controls.

Immunofluorescence of mammalian cells

For the co-localization studies, sections from the temporal cortex of DLB/PD and control cases and from αSyn tg and non-tg mice were used. Free-floating 40 mm thick vibratome sections were washed with Tris-buffered saline (TBS, pH 7.4), pre-treated in 3% H_2O_2 and blocked with 10% serum (Vector), 3% bovine serum albumin (Sigma-Aldrich) and 0.2% gelatin in TBS-Tx.

Double-immunofluorescence analyses were performed utilizing the Tyramide Signal Amplification™-Direct (Red) system (NEN Life Sciences). Specificity of this system was tested by deleting each primary antibody. For the Rab5 studies, sections were double-labeled with monoclonal antibodies against αSyn (1:20 000) (Cell Signaling) and Rab5 (1:75) (Vector) and detected with Tyramide Red and fluorescein isothiocyanate (FITC)-conjugated secondary antibodies (1:75) (Vector), respectively. For the CKIδ studies, sections were double-labeled with the polyclonal antibodies against αSyn (1:200) (Chemicon) and CKIδ (C-18) (Santa Cruz Biotechnology) and detected with FITC and Tyramid Red-conjugated secondary antibodies (1:75) (Vector), respectively. Sections were imaged with a Zeiss 63× (N.A. 1.4) objective on an Axiovert 35 microscope (Zeiss) with an attached MRC1024 laser scanning confocal microscope system (BioRad). All sections were processed simultaneously under the same conditions and experiments were performed twice for reproducibility.

Statistical analyses

Statistical analysis was performed using Prism 5 (GraphPad Software). Student's *t*-test was run for pairwise comparisons between groups at a single condition, and ANOVA for repetitive measurements was run for pairwise comparisons between groups throughout multiple treatments. Significance *P*-values were $^{*}P < 0.05$, $^{**}P < 0.01$ and $^{***}P < 0.001$.

SUPPLEMENTARY MATERIAL

Supplementary Material is available at *HMG* online.

ACKNOWLEDGEMENTS

We thank Charles Boone for kindly providing plasmids p4348 and p4339 and strain Y5563, Robert Edwards for plasmids containing S129A and S129E αSyn, and Randy Schekman for temperature-sensitive secretory mutants. Microscopy was supported by the Nikon Imaging Center (UCSF) and the Keck Microscopy Core (UW). We thank Angela Sia for contributing to the generation of pRS-derived plasmids for gamma integration. Finally, the authors thank S. Ordway and G. Howard for editorial assistance, and Robert Edwards, Flaviano Giorgini, Gregor Lotz, Robert Nussbaum, Jean Savare and Daniel Zwilling for useful discussions.

Conflict of Interest statement. None declared.

FUNDING

This work was supported by the National Institutes of Health (R01NS047237 to P.J.M. and AG022074 to P.J.M. and E.M.); the Netherlands Organization for Health Research and Development (ZonMW-VIDI-917.76.329 to F.R.); the Utrecht University (High Potential Grant to F.R.); and the Larry L. Hillblom Foundation (Fellowship Grant 2006/2T to V.S.).

REFERENCES

1. Spillantini, M.G. and Goedert, M. (2000) The alpha-synucleinopathies: Parkinson's disease, dementia with Lewy bodies, and multiple system atrophy. *Ann. NY Acad. Sci.*, **920**, 16–27.
2. Ben Gedalya, T., Loeb, V., Israeli, E., Altschuler, Y., Selkoe, D.J. and Sharon, R. (2009) Alpha-synuclein and polyunsaturated fatty acids promote clathrin-mediated endocytosis and synaptic vesicle recycling. *Traffic*, **10**, 218–234.
3. Cabin, D.E., Shimazu, K., Murphy, D., Cole, N.B., Gottschalk, W., McIlwain, K.L., Orrison, B., Chen, A., Ellis, C.E., Paylor, R. *et al.* (2002) Synaptic vesicle depletion correlates with attenuated synaptic responses to prolonged repetitive stimulation in mice lacking alpha-synuclein. *J. Neurosci.*, **22**, 8797–8807.
4. Chandra, S., Gallardo, G., Fernandez-Chacon, R., Schluter, O.M. and Sudhof, T.C. (2005) Alpha-synuclein cooperates with CSPalpha in preventing neurodegeneration. *Cell*, **123**, 383–396.
5. Liu, S., Ninan, I., Antonova, I., Battaglia, F., Trinchese, F., Narasanna, A., Kolodilov, N., Dauer, W., Hawkins, R.D. and Arancio, O. (2004) alpha-Synuclein produces a long-lasting increase in neurotransmitter release. *EMBO J.*, **23**, 4506–4516.
6. Singleton, A.B., Farrer, M., Johnson, J., Singleton, A., Hague, S., Kachergus, J., Hulihan, M., Peuralinna, T., Dutra, A., Nussbaum, R. *et al.* (2003) alpha-Synuclein locus triplication causes Parkinson's disease. *Science*, **302**, 841.
7. Fujita, Y., Ohama, E., Takatama, M., Al-Sarraj, S. and Okamoto, K. (2006) Fragmentation of Golgi apparatus of nigral neurons with alpha-synuclein-positive inclusions in patients with Parkinson's disease. *Acta Neuropathol.*, **112**, 261–265.
8. Gosavi, N., Lee, H.J., Lee, J.S., Patel, S. and Lee, S.J. (2002) Golgi fragmentation occurs in the cells with prefibrillar alpha-synuclein aggregates and precedes the formation of fibrillar inclusion. *J. Biol. Chem.*, **277**, 48984–48992.
9. Larsen, K.E., Schmitz, Y., Troyer, M.D., Mosharov, E., Dietrich, P., Quazi, A.Z., Savalle, M., Nemani, V., Chaudhry, F.A., Edwards, R.H. *et al.* (2006) Alpha-synuclein overexpression in PC12 and chromaffin cells impairs catecholamine release by interfering with a late step in exocytosis. *J. Neurosci.*, **26**, 11915–11922.
10. Lee, H.J., Khoshaghideh, F., Lee, S. and Lee, S.J. (2006) Impairment of microtubule-dependent trafficking by overexpression of alpha-synuclein. *Eur. J. Neurosci.*, **24**, 3153–3162.
11. Thayanidhi, N., Helm, J.R., Nycz, D.C., Bentley, M., Liang, Y. and Hay, J.C. (2010) Alpha-synuclein delays endoplasmic reticulum (ER)-to-Golgi transport in mammalian cells by antagonizing ER/Golgi SNAREs. *Mol. Biol. Cell*, **21**, 1850–1863.
12. Cooper, A.A., Gitler, A.D., Cashikar, A., Haynes, C.M., Hill, K.J., Bhullar, B., Liu, K., Xu, K., Strathearn, K.E., Liu, F. *et al.* (2006) Alpha-synuclein blocks ER-Golgi traffic and Rab1 rescues neuron loss in Parkinson's models. *Science*, **313**, 324–328.
13. Gitler, A.D., Bevis, B.J., Shorter, J., Strathearn, K.E., Hamamichi, S., Su, L.J., Caldwell, K.A., Caldwell, G.A., Rochet, J.C., McCaffery, J.M. *et al.* (2008) The Parkinson's disease protein alpha-synuclein disrupts cellular Rab homeostasis. *Proc. Natl Acad. Sci. USA*, **105**, 145–150.
14. Zabrocki, P., Bastiaens, I., Delay, C., Bammens, T., Ghillebert, R., Pellens, K., De Virgilio, C., Van Leuven, F. and Winderickx, J. (2008) Phosphorylation, lipid raft interaction and traffic of alpha-synuclein in a yeast model for Parkinson. *Biochim. Biophys. Acta*, **1783**, 1767–1780.
15. Soper, J.H., Roy, S., Stieber, A., Lee, E., Wilson, R.B., Trojanowski, J.Q., Burd, C.G. and Lee, V.M. (2008) Alpha-synuclein-induced aggregation of cytoplasmic vesicles in *Saccharomyces cerevisiae*. *Mol. Biol. Cell*, **19**, 1093–1103.
16. Flower, T.R., Clark-Dixon, C., Metoyer, C., Yang, H., Shi, R., Zhang, Z. and Witt, S.N. (2007) YGR198w (YPP1) targets A30P alpha-synuclein to the vacuole for degradation. *J. Cell Biol.*, **177**, 1091–1104.
17. Kuwahara, T., Koyama, A., Koyama, S., Yoshina, S., Ren, C.H., Kato, T., Mitani, S. and Iwatsubo, T. (2008) A systematic RNAi screen reveals involvement of endocytic pathway in neuronal dysfunction in alpha-synuclein transgenic *C. elegans*. *Hum. Mol. Genet.*, **17**, 2997–3009.
18. Liang, J., Clark-Dixon, C., Wang, S., Flower, T.R., Williams-Hart, T., Zweig, R., Robinson, L.C., Tatchell, K. and Witt, S.N. (2008) Novel suppressors of alpha-synuclein toxicity identified using yeast. *Hum. Mol. Genet.*, **17**, 3784–3795.
19. van Ham, T.J., Thijssen, K.L., Breitling, R., Hofstra, R.M., Plasterk, R.H. and Nollen, E.A. (2008) *C. elegans* model identifies genetic modifiers of alpha-synuclein inclusion formation during aging. *PLoS Genet.*, **4**, e1000027.
20. Willingham, S., Outeiro, T.F., DeVit, M.J., Lindquist, S.L. and Muchowski, P.J. (2003) Yeast genes that enhance the toxicity of a mutant huntingtin fragment or alpha-synuclein. *Science*, **302**, 1769–1772.
21. Fujiwara, H., Hasegawa, M., Dohmae, N., Kawashima, A., Masliah, E., Goldberg, M.S., Shen, J., Takio, K. and Iwatsubo, T. (2002) alpha-Synuclein is phosphorylated in synucleinopathy lesions. *Nat. Cell Biol.*, **4**, 160–164.
22. Waxman, E.A. and Giasson, B.I. (2008) Specificity and regulation of casein kinase-mediated phosphorylation of alpha-synuclein. *J. Neuropathol. Exp. Neurol.*, **67**, 402–416.
23. Ishii, A., Nonaka, T., Taniguchi, S., Saito, T., Arai, T., Mann, D., Iwatsubo, T., Hisanaga, S., Goedert, M. and Hasegawa, M. (2007) Casein kinase 2 is the major enzyme in brain that phosphorylates Ser129 of human alpha-synuclein: implication for alpha-synucleinopathies. *FEBS Lett.*, **581**, 4711–4717.
24. Okochi, M., Walter, J., Koyama, A., Nakajo, S., Baba, M., Iwatsubo, T., Meijer, L., Kahle, P.J. and Haass, C. (2000) Constitutive phosphorylation of the Parkinson's disease associated alpha-synuclein. *J. Biol. Chem.*, **275**, 390–397.
25. Inglis, K.J., Chereau, D., Brigham, E.F., Chiou, S.S., Schobel, S., Frigon, N.L., Yu, M., Caccavello, R.J., Nelson, S., Motter, R. *et al.* (2009) Polo-like kinase 2 (PLK2) phosphorylates alpha-synuclein at serine 129 in central nervous system. *J. Biol. Chem.*, **284**, 2598–2602.
26. Pronin, A.N., Morris, A.J., Surguchov, A. and Benovic, J.L. (2000) Synucleins are a novel class of substrates for G protein-coupled receptor kinases. *J. Biol. Chem.*, **275**, 26515–26522.
27. Qing, H., Wong, W., McGeer, E.G. and McGeer, P.L. (2009) Lrrk2 phosphorylates alpha synuclein at serine 129: Parkinson disease implications. *Biochem. Biophys. Res. Commun.*, **387**, 149–152.
28. Sakamoto, M., Arawaka, S., Hara, S., Sato, H., Cui, C., Machiya, Y., Koyama, S., Wada, M., Kawanami, T., Kurita, K. *et al.* (2009) Contribution of endogenous G-protein-coupled receptor kinases to Ser129 phosphorylation of alpha-synuclein in HEK293 cells. *Biochem. Biophys. Res. Commun.*, **384**, 378–382.
29. Azeredo da Silveira, S., Schneider, B.L., Cifuentes-Diaz, C., Sage, D., Abbas-Terki, T., Iwatsubo, T., Unser, M. and Aebischer, P. (2009) Phosphorylation does not prompt, nor prevent, the formation of

alpha-synuclein toxic species in a rat model of Parkinson's disease. *Hum. Mol. Genet.*, **18**, 872–887.
30. Chen, L. and Feany, M.B. (2005) Alpha-synuclein phosphorylation controls neurotoxicity and inclusion formation in a *Drosophila* model of Parkinson disease. *Nat. Neurosci.*, **8**, 657–663.
31. Gorbatyuk, O.S., Li, S., Sullivan, L.F., Chen, W., Kondrikova, G., Manfredsson, F.P., Mandel, R.J. and Muzyczka, N. (2008) The phosphorylation state of Ser-129 in human alpha-synuclein determines neurodegeneration in a rat model of Parkinson disease. *Proc. Natl Acad. Sci. USA*, **105**, 763–768.
32. McFarland, N.R., Fan, Z., Xu, K., Schwarzschild, M.A., Feany, M.B., Hyman, B.T. and McLean, P.J. (2009) Alpha-synuclein S129 phosphorylation mutants do not alter nigrostriatal toxicity in a rat model of Parkinson disease. *J. Neuropathol. Exp. Neurol.*, **68**, 515–524.
33. Outeiro, T.F. and Lindquist, S. (2003) Yeast cells provide insight into alpha-synuclein biology and pathobiology. *Science*, **302**, 1772–1775.
34. Lewis, M.J., Nichols, B.J., Prescianotto-Baschong, C., Riezman, H. and Pelham, H.R. (2000) Specific retrieval of the exocytic SNARE Snc1p from early yeast endosomes. *Mol. Biol. Cell*, **11**, 23–38.
35. Reggiori, F., Black, M.W. and Pelham, H.R. (2000) Polar transmembrane domains target proteins to the interior of the yeast vacuole. *Mol. Biol. Cell*, **11**, 3737–3749.
36. Reggiori, F. and Pelham, H.R. (2001) Sorting of proteins into multivesicular bodies: ubiquitin-dependent and -independent targeting. *EMBO J.*, **20**, 5176–5186.
37. Marchal, C., Dupre, S. and Urban-Grimal, D. (2002) Casein kinase I controls a late step in the endocytic trafficking of yeast uracil permease. *J. Cell Sci.*, **115**, 217–226.
38. Marchal, C., Haguenauer-Tsapis, R. and Urban-Grimal, D. (2000) Casein kinase I-dependent phosphorylation within a PEST sequence and ubiquitination at nearby lysines signal endocytosis of yeast uracil permease. *J. Biol. Chem.*, **275**, 23608–23614.
39. Panek, H.R., Conibear, E., Bryan, J.D., Colvin, R.T., Goshorn, C.D. and Robinson, L.C. (2000) Identification of Rgp1p, a novel Golgi recycling factor, as a protein required for efficient localization of yeast casein kinase 1 to the plasma membrane. *J. Cell Sci.*, **113**, 4545–4555.
40. Rose, K., Rudge, S.A., Frohman, M.A., Morris, A.J. and Engebrecht, J. (1995) Phospholipase D signaling is essential for meiosis. *Proc. Natl Acad. Sci. USA*, **92**, 12151–12155.
41. Chau, K.Y., Ching, H.L., Schapira, A.H. and Cooper, J.M. (2009) Relationship between alpha synuclein phosphorylation, proteasomal inhibition and cell death: relevance to Parkinson's disease pathogenesis. *J. Neurochem.*, **110**, 1005–1013.
42. Kragh, C.L., Lund, L.B., Febbraro, F., Hansen, H.D., Gai, W.P., El-Agnaf, O., Richter-Landsberg, C. and Jensen, P.H. (2009) {alpha}-Synuclein aggregation and Ser-129 phosphorylation-dependent cell death in oligodendroglial cells. *J. Biol. Chem.*, **284**, 10211–10222.
43. Chen, D.C., Yang, B.C. and Kuo, T.T. (1992) One-step transformation of yeast in stationary phase. *Curr. Genet.*, **21**, 83–84.
44. Veal, E.A., Ross, S.J., Malakasi, P., Peacock, E. and Morgan, B.A. (2003) Ybp1 is required for the hydrogen peroxide-induced oxidation of the Yap1 transcription factor. *J. Biol. Chem.*, **278**, 30896–30904.
45. Witt, S.N. and Flower, T.R. (2006) alpha-Synuclein, oxidative stress and apoptosis from the perspective of a yeast model of Parkinson's disease. *FEMS Yeast Res.*, **6**, 1107–1116.
46. Masliah, E., Rockenstein, E., Veinbergs, I., Mallory, M., Hashimoto, M., Takeda, A., Sagara, Y., Sisk, A. and Mucke, L. (2000) Dopaminergic loss and inclusion body formation in alpha-synuclein mice: implications for neurodegenerative disorders. *Science*, **287**, 1265–1269.
47. Rockenstein, E., Mallory, M., Mante, M., Sisk, A. and Masliaha, E. (2001) Early formation of mature amyloid-beta protein deposits in a mutant APP transgenic model depends on levels of Abeta(1-42). *J. Neurosci. Res.*, **66**, 573–582.
48. Milne, D.M., Looby, P. and Meek, D.W. (2001) Catalytic activity of protein kinase CK1 delta (casein kinase 1delta) is essential for its normal subcellular localization. *Exp. Cell Res.*, **263**, 43–54.
49. Yu, S. and Roth, M.G. (2002) Casein kinase I regulates membrane binding by ARF GAP1. *Mol. Biol. Cell*, **13**, 2559–2570.
50. Yasojima, K., Kuret, J., DeMaggio, A.J., McGeer, E. and McGeer, P.L. (2000) Casein kinase 1 delta mRNA is upregulated in Alzheimer disease brain. *Brain Res.*, **865**, 116–120.
51. Darios, F., Ruiperez, V., Lopez, I., Villanueva, J., Gutierrez, L.M. and Davletov, B. (2010) Alpha-Synuclein sequesters arachidonic acid to modulate SNARE-mediated exocytosis. *EMBO Rep.*, **11**, 528–533.
52. Garcia-Reitbock, P., Anichtchik, O., Bellucci, A., Iovino, M., Ballini, C., Fineberg, E., Ghetti, B., Della Corte, R., Spano, P., Tofaris, G.K., Goedert, M. and Spillantini, M.G. (2010) SNARE protein redistribution and synaptic failure in a transgenic mouse model of Parkinson's disease. *Brain*, **133**, 2032–2044.
53. Mumberg, D., Muller, R. and Funk, M. (1994) Regulatable promoters of *Saccharomyces cerevisiae*: comparison of transcriptional activity and their use for heterologous expression. *Nucleic Acids Res.*, **22**, 5767–5768.
54. Mumberg, D., Muller, R. and Funk, M. (1995) Yeast vectors for the controlled expression of heterologous proteins in different genetic backgrounds. *Gene*, **156**, 119–122.
55. Lafourcade, C., Galan, J.M., Gloor, Y., Haguenauer-Tsapis, R. and Peter, M. (2004) The GTPase-activating enzyme Gyp1p is required for recycling of internalized membrane material by inactivation of the Rab/Ypt GTPase Ypt1p. *Mol. Cell. Biol.*, **24**, 3815–3826.
56. Luo, Z. and Gallwitz, D. (2003) Biochemical and genetic evidence for the involvement of yeast Ypt6-GTPase in protein retrieval to different Golgi compartments. *J. Biol. Chem.*, **278**, 791–799.
57. Dalfo, E., Barrachina, M., Rosa, J.L., Ambrosio, S. and Ferrer, I. (2004) Abnormal alpha-synuclein interactions with rab3a and rabphilin in diffuse Lewy body disease. *Neurobiol. Dis.*, **16**, 92–97.
58. Dalfo, E. and Ferrer, I. (2005) Alpha-synuclein binding to rab3a in multiple system atrophy. *Neurosci. Lett.*, **380**, 170–175.
59. Nakamura, S., Kawamoto, Y., Nakano, S. and Akiguchi, I. (2000) Expression of the endocytosis regulatory proteins Rab5 and Rabaptin-5 in glial cytoplasmic inclusions from brains with multiple system atrophy. *Clin. Neuropathol.*, **19**, 51–56.
60. Forno, L.S. and Norville, R.L. (1976) Ultrastructure of Lewy bodies in the stellate ganglion. *Acta Neuropathol.*, **34**, 183–197.
61. Watanabe, I., Vachal, E. and Tomita, T. (1977) Dense core vesicles around the Lewy body in incidental Parkinson's disease: an electron microscopic study. *Acta Neuropathol.*, **39**, 173–175.
62. Stenmark, H. and Olkkonen, V.M. (2001) The Rab GTPase family. *Genome Biol.*, **2**, REVIEWS3007.
63. van der Sluijs, P., Hull, M., Webster, P., Male, P., Goud, B. and Mellman, I. (1992) The small GTP-binding protein rab4 controls an early sorting event on the endocytic pathway. *Cell*, **70**, 729–740.
64. Simonsen, A., Lippe, R., Christoforidis, S., Gaullier, J.M., Brech, A., Callaghan, J., Toh, B.H., Murphy, C., Zerial, M. and Stenmark, H. (1998) EEA1 links PI(3)K function to Rab5 regulation of endosome fusion. *Nature*, **394**, 494–498.
65. Stenmark, H., Parton, R.G., Steele-Mortimer, O., Lutcke, A., Gruenberg, J. and Zerial, M. (1994) Inhibition of rab5 GTPase activity stimulates membrane fusion in endocytosis. *EMBO J.*, **13**, 1287–1296.
66. Hirai, Y., Fujita, S.C., Iwatsubo, T. and Hasegawa, M. (2004) Phosphorylated alpha-synuclein in normal mouse brain. *FEBS Lett.*, **572**, 227–232.
67. Flower, T.R., Chesnokova, L.S., Froelich, C.A., Dixon, C. and Witt, S.N. (2005) Heat shock prevents alpha-synuclein-induced apoptosis in a yeast model of Parkinson's disease. *J. Mol. Biol.*, **351**, 1081–1100.
68. Griffioen, G., Duhamel, H., Van Damme, N., Pellens, K., Zabrocki, P., Pannecouque, C., van Leuven, F., Winderickx, J. and Wera, S. (2006) A yeast-based model of alpha-synucleinopathy identifies compounds with therapeutic potential. *Biochim. Biophys. Acta*, **1762**, 312–318.
69. Faundez, V.V. and Kelly, R.B. (2000) The AP-3 complex required for endosomal synaptic vesicle biogenesis is associated with a casein kinase Ialpha-like isoform. *Mol. Biol. Cell*, **11**, 2591–2604.
70. Bennett, M.K., Miller, K.G. and Scheller, R.H. (1993) Casein kinase II phosphorylates the synaptic vesicle protein p65. *J. Neurosci.*, **13**, 1701–1707.
71. Davletov, B., Sontag, J.M., Hata, Y., Petrenko, A.G., Fykse, E.M., Jahn, R. and Sudhof, T.C. (1993) Phosphorylation of synaptotagmin I by casein kinase II. *J. Biol. Chem.*, **268**, 6816–6822.
72. Krantz, D.E., Peter, D., Liu, Y. and Edwards, R.H. (1997) Phosphorylation of a vesicular monoamine transporter by casein kinase II. *J. Biol. Chem.*, **272**, 6752–6759.
73. Sikorski, R.S. and Hieter, P. (1989) A system of shuttle vectors and yeast host strains designed for efficient manipulation of DNA in *Saccharomyces cerevisiae*. *Genetics*, **122**, 19–27.
74. Mari, M., Griffith, J., Rieter, E., Krisnappa, L., Klionsky, D.J. and Reggiori, F. (2010) An Atg9-containing compartment that functions

in the early steps of autophagosome biogenesis. *J. Cell Biol.*, **190**, 1005–1022.
75. Brachmann, C.B., Davies, A., Cost, G.J., Caputo, E., Li, J., Hieter, P. and Boeke, J.D. (1998) Designer deletion strains derived from *Saccharomyces cerevisiae* S288C: a useful set of strains and plasmids for PCR-mediated gene disruption and other applications. *Yeast*, **14**, 115–132.
76. Tong, A.H., Evangelista, M., Parsons, A.B., Xu, H., Bader, G.D., Page, N., Robinson, M., Raghibizadeh, S., Hogue, C.W., Bussey, H. *et al.* (2001) Systematic genetic analysis with ordered arrays of yeast deletion mutants. *Science*, **294**, 2364–2368.
77. Gietz, R.D., Schiestl, R.H., Willems, A.R. and Woods, R.A. (1995) Studies on the transformation of intact yeast cells by the LiAc/SS-DNA/PEG procedure. *Yeast*, **11**, 355–360.
78. Masliah, E., Rockenstein, E., Adame, A., Alford, M., Crews, L., Hashimoto, M., Seubert, P., Lee, M., Goldstein, J., Chilcote, T. *et al.* (2005) Effects of alpha-synuclein immunization in a mouse model of Parkinson's disease. *Neuron*, **46**, 857–868.
79. Masliah, E., Rockenstein, E., Veinbergs, I., Sagara, Y., Mallory, M., Hashimoto, M. and Mucke, L. (2001) Beta-amyloid peptides enhance alpha-synuclein accumulation and neuronal deficits in a transgenic mouse model linking Alzheimer's disease and Parkinson's disease. *Proc. Natl Acad. Sci. USA*, **98**, 12245–12250.
80. Rockenstein, E., Mallory, M., Hashimoto, M., Song, D., Shults, C.W., Lang, I. and Masliah, E. (2002) Differential neuropathological alterations in transgenic mice expressing alpha-synuclein from the platelet-derived growth factor and Thy-1 promoters. *J. Neurosci. Res.*, **68**, 568–578.
81. Hansen, L.A., Daniel, S.E., Wilcock, G.K. and Love, S. (1998) Frontal cortical synaptophysin in Lewy body diseases: relation to Alzheimer's disease and dementia. *J. Neurol. Neurosurg. Psychiatry*, **64**, 653–656.
82. Hansen, L.A., Masliah, E., Quijada-Fawcett, S. and Rexin, D. (1991) Entorhinal neurofibrillary tangles in Alzheimer disease with Lewy bodies. *Neurosci. Lett.*, **129**, 269–272.
83. Braak, H. and Braak, E. (1991) Morphological changes in the human cerebral cortex in dementia. *J. Hirnforsch.*, **32**, 277–282.
84. McKeith, I.G., Galasko, D., Kosaka, K., Perry, E.K., Dickson, D.W., Hansen, L.A., Salmon, D.P., Lowe, J., Mirra, S.S., Byrne, E.J. *et al.* (1996) Consensus guidelines for the clinical and pathologic diagnosis of dementia with Lewy bodies (DLB): report of the consortium on DLB international workshop. *Neurology*, **47**, 1113–1124.
85. Griffith, J., Mari, M., De Maziere, A. and Reggiori, F. (2008) A cryosectioning procedure for the ultrastructural analysis and the immunogold labelling of yeast *Saccharomyces cerevisiae*. *Traffic*, **9**, 1060–1072.
86. Slot, J.W. and Geuze, H.J. (2007) Cryosectioning and immunolabeling. *Nat. Protoc.*, **2**, 2480–2491.
87. Giaever, G., Chu, A.M., Ni, L., Connelly, C., Riles, L., Veronneau, S., Dow, S., Lucau-Danila, A., Anderson, K., Andre, B. *et al.* (2002) Functional profiling of the *Saccharomyces cerevisiae* genome. *Nature*, **418**, 387–391.
88. Novick, P., Field, C. and Schekman, R. (1980) Identification of 23 complementation groups required for post-translational events in the yeast secretory pathway. *Cell*, **21**, 205–215.
89. Thomas, B.J. and Rothstein, R. (1989) The genetic control of direct-repeat recombination in *Saccharomyces*: the effect of rad52 and rad1 on mitotic recombination at GAL10, a transcriptionally regulated gene. *Genetics*, **123**, 725–738.